# Process Analysis of Chemical Looping Gasification of Biomass for Fischer-Tropsch Crude Production with Net-Negative

(article starts on next page)

# Process Analysis of Chemical Looping Gasification of Biomass for Fischer−Tropsch Crude Production with Net-Negative CO₂ Emissions: Part 1

Tharun Roshan Kumar,* Tobias Mattisson, Magnus Rydén, and Viktor Stenberg

Read Online

ACCESS | Metrics & More | Article Recommendations | SI Supporting Information

**ABSTRACT:** Large-scale biofuel production plants require an efficient gasification process that generates syngas of high quality (with minimal gas contaminants and inert gases) to minimize the extent of the syngas cleaning processes required for liquid biofuel production. This work presents process modeling of the chemical looping gasification (CLG) process for syngas production. The CLG process is integrated with a Fischer−Tropsch synthesis (FTS) process to produce Fischer−Tropsch (FT) crude with net-negative CO₂ emissions, enabling process and system-level analyses of this novel biomass-to-liquid process. CLG resembles indirect gasification in an interconnected circulating fluidized bed reactor, where instead of inert bed material, a solid-oxygen carrier, such as mineral ores rich in iron or manganese oxides, is used. The oxygen carrier particles undergo oxidation and reduction in the air reactor and fuel reactor, respectively, thereby providing heat and oxygen for gasification. This work uses data from CLG experiments performed with steel converter slag as the oxygen carrier and investigates its potential when integrated with different downstream gas cleaning trains and the subsequent fuel synthesis process with the primary objective of quantifying and evaluating the performance of the integrated CLG−FT process plant. Syngas with a high energy content of 12 MJ/Nm³ (lower heating value basis) is predicted with a cold gas efficiency of 73%. CO₂/CO ratios, higher than indirect biomass gasification, are also predicted in the raw syngas produced; thus, there exists an opportunity to capture biogenic CO₂ with a relatively lower energy penalty in the subsequent gas cleaning stages. This work quantifies other key performance indicators, such as heat recovery potential, negative CO₂ emission capacity, and FT crude production efficiency of the CLG−FT plant. A 100 MW_th CLG plant produces roughly 677−696 barrels per day of FT crude, with net-negative emissions of roughly 180 kilotonnes of CO₂ annually.
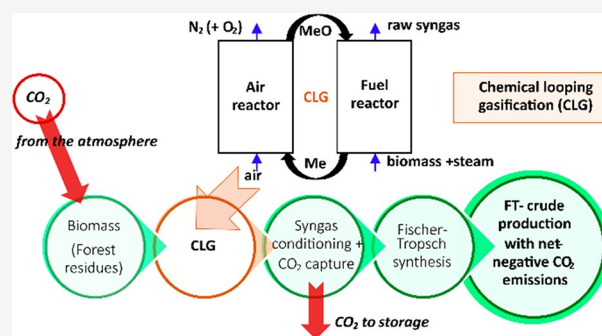
## 1. INTRODUCTION

Transport biofuels are one of the promising pathways to decarbonize the transportation sector, especially hard-to-abate sectors, such as aviation or maritime transportation. Switching to biofuels could be a way of reducing carbon dioxide emissions but also reducing dependence upon crude oil imports. The latter is important with respect to energy security and price stability. Biofuel could potentially make up a third of the total transport fuel demand by 2050, according to the International Energy Agency (IEA).[1] There are, however, concerns over its impact on land-use change and its plausible effect on food prices that makes it imperative to use sustainable biomass, such as waste streams from agriculture and forests. These waste streams could be used to produce advanced biofuels, such as synthetic natural gas (SNG), and liquid biofuels, such as methanol or Fischer−Tropsch (FT) crude from the Fischer−Tropsch synthesis (FTS) process.

Chemical looping gasification (CLG) of biomass is a novel gasification technology for high-quality syngas production for utilization in the downstream fuel synthesis process, with its inherent advantage of restricting CO₂ to the product gas stream. The CLG process is similar to the indirect gasification (IG) process[2] for syngas production, where the advantages arise from replacing the inert bed material in the IG process with oxygen carrier (OC) particles. The OC particles not only provide parts of oxygen required for gasification but also act as the heat carrier in the process, where the heat required in the gasifier is provided through cyclic oxidation of reduced OC particles with air in the air reactor (AR). With OC particles employed in an interconnected circulating fluidized bed (CFB) system, fuel−air mixing is avoided, resulting in two separate gas streams, i.e., raw syngas from the fuel reactor (FR) with minimal nitrogen dilution and oxygen-depleted air from the
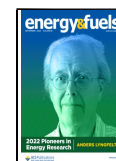
AR. The resulting oxygen-depleted air stream from the AR would ideally be cooled to ambient temperatures for heat recovery, as it is free of gas contaminants. In comparison to the IG process, in CLG, ideally, most $CO_2$ is restricted to the FR, where it is available for carbon capture. In comparison to the IG process, the partial pressure of $CO_2$ would be higher and the volumes of diluents and tars would be lower. Therefore, CLG would allow for reduced costs related to carbon sequestration and gas cleaning.

The aim of this study is to develop a steady-state process model of CLG, using a steel industry byproduct, Linz–Donawitz (LD) slag, as the primary OC in the process. Further, the CLG model is integrated with a downstream FTS process model to evaluate the overall process efficiencies and estimate the carbon capture and fuel production capacity of the integrated plant. The effect of operating parameters, such as steam/biomass ratio, gasification temperature, and pressure, is investigated. In addition to this, different process configurations of the gas cleaning train are explored.

## 2. BACKGROUND

**2.1. CLG.** The CLG process is based on chemical looping combustion (CLC), a technology where gaseous and solid fuels are combusted in an interconnected CFB, assisted with OCs in the form of metal oxide particles, as the bed material in the FR.[3,4] The OC is reduced in the FR and, thereby, provides elemental oxygen required for combustion. In a separate reactor, referred to as the AR, the reduced OC is oxidized with air. Direct fuel and air mixing is avoided by this measure of cyclic oxidation–reduction of the metal oxide particles in two separate reactors, which results in an oxygen-depleted air stream from the AR and a flue gas concentrated with $CO_2$ from the FR. CLC is estimated to considerably bring down costs associated with carbon capture and storage,[5] mainly by avoiding monetary and energy costs related to gas separation. Net-negative emissions could be achieved through CLC of biomass with $CO_2$ storage. This could potentially be a method to remove $CO_2$ from the atmosphere at a low cost. CLG uses the same fundamental principles as CLC, but the primary objective is to gasify solid fuels to syngas, as shown in Figure 1.

Table 1 lists reactions associated with syngas generation via reduction of the OC particles in the FR and oxidation of the reduced OC with air in the AR.
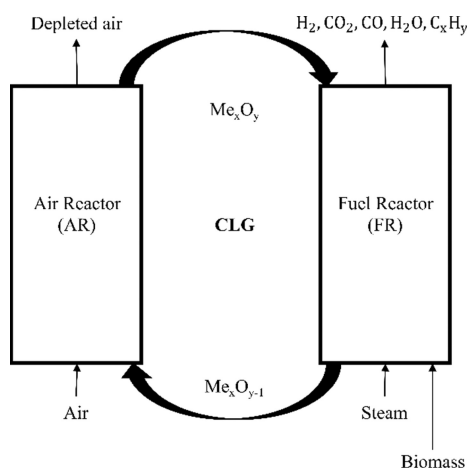


**Figure 1.** Schematic of CLG of biomass.

In CLG, complete oxidation of fuel is undesirable, unlike the CLC process, where the main objective is to achieve high fuel conversions in the FR through sufficient oxygen transport and solids circulation. In CLG, the primary objective is to produce high-quality syngas through partial oxidation of the fuel in the FR. Still, in CLG, it is necessary and expected that some of the fuel is oxidized to $CO_2$ and $H_2O$, in addition to CO and $H_2$. Both of the processes have the inherent ability to restrict $CO_2$ only to the FR and achieve high carbon conversions in it, thereby significantly reducing the additional effort required to capture $CO_2$ downstream compared to conventional solid fuel combustion or gasification processes. The syngas composition would, however, depend upon various parameters, such as the type of fuel, the OC used in the reactors, and the operating conditions in the FR. The gases produced in the gasification process in CLG mainly consist of $H_2$, CO, $CO_2$, and $H_2O$, along with gas contaminants, such as hydrogen sulfide, ammonia, and other tar components, also expected to be present along with the product gas. The $CO_2/CO$ ratio is expected to be higher in CLG when compared to the indirect gasification process as a result of the more oxidizing environment in the FR, and this is also expected to limit tar formation in the FR. Further, replacing the inert bed material with OCs could potentially have added benefits, such as the catalytic activity toward tar destruction, improved rates of char gasification as a result of lattice oxygen uncoupling, and reducing the concentration of species that inhibit char gasification rates.[6−8]

CLG operations are highly dependent upon the type and nature of OC used in the process because it requires an optimal balance between partial oxidation of fuel for high-quality syngas production while at the same time achieving an autothermal operation. In the recent past, CLG has been experimentally evaluated using different types of fuel, OCs, and different reactor setups.[9−11] Chemical looping systems with a Cu−Mg−Si-based OC were investigated by Jin et al.[12] with a focus on evaluating the energy performance and challenges associated with maintaining an autothermal operation in such units. Pissot et al.[11] investigated CLG with LD slag, employing various strategies, such as adjusting the overall oxidation state of the bed material and dilution of the OC carrier with inert bed material, to name a few. CLG of rice husk was investigated by Ge et al.[10] with natural hematite as the OC in a 25 kW BFB reactor, where it was demonstrated that stable CLG operation was attained with 40% hematite and 60% sand, by weight, in the bed material. Further, newer methods to control the oxygen/fuel ratio ($\lambda$) and decouple the oxygen and heat transport between the FR and AR have also been demonstrated for CLG of biomass with ilmenite in a 1.5 $kW_{th}$ unit by Condori et al.[13] Other CLG investigations include gasification of pine sawdust in a dual fluidized bed (DFB) gasifier with iron ore as the OC for hydrogen production[14] and CLG of pine sawdust in a BFB gasifier with $Fe_2O_3/Al_2O_3$ (70:30% by weight) as the OC, where a carbon conversion efficiency of 89% was reported.[15] CLG of high-sulfur petroleum coke was investigated by Shen et al.,[16] with hematite as the OC, that indicated a carbon conversion of roughly 70%. CLG operation in the 10 kW Chalmers unit with high-volatile fuel, such as white wood pellets and black wood pellets with LD slag as the OC was investigated by Moldenhauer et al.,[17] where the estimated raw gas composition mainly comprised of $H_2$, $CO_2$, CO, and $CH_4$ in that order. In a more recently published work by Condori et al.,[18] CLG

**Table 1. Reactions Associated with OC Particles in FR and AR**

| unit | reaction |
|---|---|
| FR | $C_nH_{2m}O_p + (n - p)Me_xO_y \rightarrow nCO + mH_2 + (n - p)Me_xO_{y-1}$ (R1) |
| AR | $O_2 + 2Me_xO_{y-1} \rightarrow 2Me_xO_y$ (R2) |

experiments were performed on industrial wood pellets and other agricultural wastes in a 1.5 kW$_{th}$ unit with LD slag, where gas compositions were estimated for different operating conditions (varied temperatures, steam/biomass ratios, and oxygen/biomass ratios and different gasification agents). Here, with steam as the gasification agent, the reported gas compositions (vol %, dry and $N_2$-free basis) were in a wide range of $H_2$ (25−40%), $CO_2$ (20−46%), CO (18−40%), and $CH_4$ (8−9%), indicating the influence of different operating conditions. Available experimental data indicate that a high-quality syngas is attainable in the CLG process that could be used for further downstream fuel synthesis processes.[19] The aforementioned research lists recent CLG experimental work performed with different types of biomass and potential OCs. However, there have been few investigations performed on modeling and integrating CLG with different fuel synthesis processes of interest that would establish the future potential of CLG in comparison to competing biomass-to-liquid fuel production routes, and this work aims to fill this specific gap.

The main reactions (eqs R3−R6) associated with biomass gasification are shown in Table 2, including their standard enthalpy of reaction.

**Table 2. Main Chemical Reactions Associated with Biomass Gasification**

| reaction name | reaction | standard enthalpy of reaction (at 298 K and 1 bar), $\Delta H$ (kJ/mol) |
|---|---|---|
| char−steam gasification | $C + H_2O \rightarrow CO + H_2$ (R3) | +131 |
| Boudouard | $C + CO_2 \rightarrow 2CO$ (R4) | +172 |
| hydrogasification | $C + 2H_2 \rightarrow CH_4$ (R5) | −74.8 |
| water−gas shift | $CO + H_2O \leftrightarrows CO_2 + H_2$ (R6) | −41.2 |

The char−steam gasification reaction and water−gas shift reaction (eqs R3 and R6) in Table 2 can be combined and written as one equation for char gasification with a mechanism factor $\alpha$, as shown in eq R8 in Table 3. This factor was estimated to range from 1.5 to 1.1 for temperatures ranging from 750 to 900 °C, respectively.[20] First, biomass devolatilizes into solid char, tar, and volatile gases, as shown in eq R7 in Table 3, followed by steam gasification of char, gas−solid reactions between the volatiles and the OC, solid−solid reactions, and tar decomposition.

OCs provide lattice oxygen for gasification, which is more likely to partially oxidize the fuel rather than fully oxidize it, as compared to gas-phase oxygen.[10] Volatile gases, mainly consisting of $H_2$, CO, and $CH_4$, produced through devolatilization, react with the solid OC particles in the FR. Equation R9 in Table 3 shows the gas−solid reaction, where volatile combustion is expected, owing to the good contact between the gases and the OC and also as a result of the redox properties of the latter.[21] Tars generally decompose into lighter hydrocarbons at high reactor temperatures and the presence of OCs, such as $Fe_2O_3$,[10,22] shown in eq R10. As per eq R11, the char fraction undergoes a solid−solid reaction by reacting with the OC particles; however, it is reported to be minimal, owing to insufficient contact between the two in a fluidized bed gasifier system, and steam as a gasifying agent is deemed to be necessary for improved char conversion in the FR.[23,24] In addition to this, $CO_2$ could also be used along with steam for fluidization through flue gas recirculation. Carbon dioxide could also act as a gasifying agent, but this is not considered in this work. Thus, the most applicable reaction (eq R8) is considered for the conversion of char (C) in the FR.

**2.2. Syngas Cleaning and Conditioning.** Gas contaminants, such as sulfur and nitrogen compounds, alkali compounds, tars, and particulate matter, are expected in the syngas from a gasification process that would need extensive cleaning before it is used. Syngas cleanup technologies have been extensively reviewed by Woolcock et al.,[25] where different gas cleaning technologies are categorized on the basis of their range of operating temperatures. In comparison to hot-gas cleanup (HGCU) and warm-gas cleanup technologies, cold-gas cleanup (CGCU) technology is mostly considered a conventional cleanup approach because of its demonstrated removal efficiency and reliability.[26] Although reliable, it is known to impact the thermal efficiency of the overall process plant as a result of lower operating temperatures.[25] Tars can either be cracked at high temperatures or scrubbed from the raw syngas using rapeseed methyl ester (RME) as the scrubbing liquid. The latter was used in the Güssing gasification plant and the Gothenburg Biomass Gasification (GoBiGas) plant.[27,28] The RME consumption in the latter, however, accounted for nearly 5−10% of the total operational cost.[27] Acid gases, such as $H_2S$ and $CO_2$, are removed by either chemical or physical

**Table 3. Main Chemical Reactions in the FR**

| reaction name | reaction |
|---|---|
| biomass devolatilization | $C_nH_{2m}O_p \rightarrow char + volatiles (CO, H_2, CO_2, CH_4, C_nH_{2m}) + tar$ (R7) |
| combined equation | $C + \alpha H_2O \rightarrow (2 - \alpha)CO + (\alpha - 1)CO_2 + \alpha H_2$ (R8) |
| gas−solid reaction | $(H_2, CO, CH_4) + nMe_xO_y \rightarrow nMe_xO_{y-1} + H_2O + CO_2$ (R9) |
| tar decomposition | $tar \rightarrow H_2 + CO + hydrocarbons (C_2, C_4, ...)$ (R10) |
| solid−solid reaction | $char + 2Me_xO_y \rightarrow 2Me_xO_{y-1} + CO_2$ (R11) |

regenerative solvents,[25,26] although acid gas removal (AGR) processes with chemical solvents, such as amines, tend to be cheaper compared to AGR processes with physical solvents. The latter is, however, preferred if the objective is to use the syngas for a fuel synthesis process that typically has stricter cleaning requirements.[25] Similar, AGR units have been modeled and investigated in a typical biomass-to-liquid fuel process chain; for example, a Selexol-based AGR unit was employed in a bio-2-DME process by Wodołażski et al.[29] In addition, this is also an important step in capturing carbon dioxide to achieve net-negative $CO_2$ emissions from the process. Fuel-bound nitrogen typically becomes converted to mainly $NH_3$ and $N_2$[30] in the conventional gasification process. In CLG, although nitrogen dilution of syngas by air is avoided, fuel-bound nitrogen in the biomass is expected to become converted to ammonia and other $NO_x$ compounds as a result of the likely oxidation of ammonia by the OCs in the FR. FTS demands syngas of high purity, thereby making the choice of the gas cleaning train and equipment vital to the overall process chain.

**2.3. FTS.** In FTS, cleaned syngas rich in hydrogen and carbon monoxide is used and upgraded to a range of long-chained hydrocarbons using supported metal catalysts, such as a cobalt- or iron-based catalyst.[31,32] The exothermic reactions (eqs R12–R14) involving FTS are shown in Table 4, where syngas becomes converted to paraffins, olefins, and alcohols.

**Table 4. Main FTS Reactions**

| reaction |
|---|
| $nCO + (2n + 1)H_2 \rightarrow C_nH_{2n+2} + nH_2O$    (R12) |
| $nCO + 2nH_2 \rightarrow C_nH_{2n} + nH_2O$    (R13) |
| $nCO + 2nH_2 \rightarrow C_nH_{2n+1}OH + (n - 1)H_2O$    (R14) |

These long-chained hydrocarbons can be further upgraded to transportation fuels and other valuable chemical products through product upgradation steps. FTS has two main operating modes, low-temperature Fischer–Tropsch (LTFT) mode and high-temperature Fischer–Tropsch (HTFT) mode. LTFT (200–240 °C) is suitable for the production of diesel and wax hydrocarbons, and HTFT (300–360 °C) is suitable for gasoline and middle-distillate hydrocarbons.[31,32] More information on catalysts used and reactor types used in FTS can be found elsewhere.[32,33] Syngas produced via biomass gasification would yield a wide range of FT products, such as biomass-derived kerosene, as either a blending component or on-specification fuel[34] suitable for decarbonizing the aviation and maritime sector. In addition, other higher value chemicals, such as bio-olefins, are also produced, which could aid in limiting the extraction of fossil-based feedstock for existing olefin production plants and also aid in offsetting carbon leakage in future olefin production plants with circular use of plastics.[35]

## 3. CASE DESCRIPTION

This work aims to establish the feasibility of using CLG together with FT crude synthesis. This was achieved by conducting process simulations of the entire process chain and establishing efficiencies and possibilities for achieving negative $CO_2$ emissions. Two different cases for FT crude production with CLG as the primary gasification technology was investigated. The CLG model in both cases was sized to 100 $MW_{th}$ input of dried biomass. Case CG with a CGCU train has two AGR units, i.e., an amine-based scrubber in the gas cleaning section and a Rectisol unit in the FTS section. In case CG, the CLG process operates at ambient pressures that require compression of the raw syngas prior to $CO_2$ capture in the two AGR units. From an economic perspective, it is pertinent to optimize this process configuration. Thus, case HG was modeled with a HGCU train for the gas cleaning section that uses a sour water–gas shift reactor, resistant to sulfur and other gas impurities, followed by tar removal and the Rectisol unit. The CLG model, in this case, is operating at an
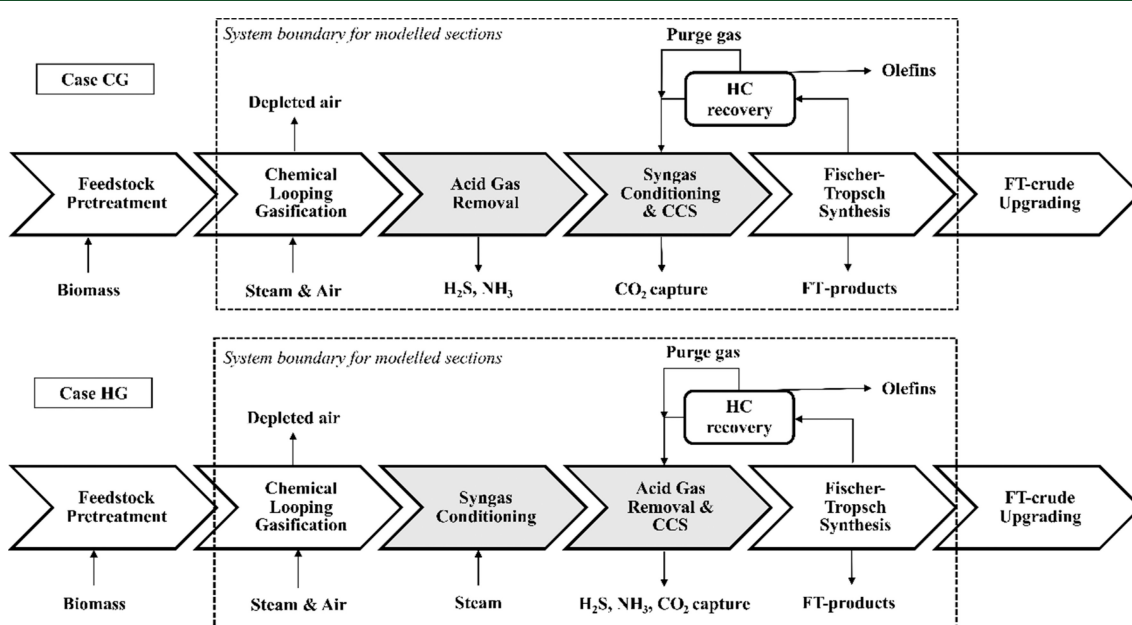


**Figure 2.** Simple schematic of cases CG and HG modeled, with the shaded stage indicating the differences between the two cases. The feedstock pretreatment and product upgrading have not been modeled in this work.

**Table 5. Summary of Feed Streams, Assumptions, and Process Conditions in the Three Sections of the CLG−FT Process Chain, Common to Both Cases CG and HG**

| Feed Streams | | | | | |
|---|---|---|---|---|---|
| fuel | forest residues | | | | |

| fuel ultimate analysis (%, w/w, dry basis) | C | H | O | N | S | ash |
|---|---|---|---|---|---|---|
| | 51.3 | 6.1 | 40.85 | 0.40 | 0.02 | 1.33 |

| fuel proximate analysis (%, w/w, dry basis) | moisture content | volatile matter | fixed carbon | ash |
|---|---|---|---|---|
| | 6 | 79.3 | 19.37 | 1.33 |

| | |
|---|---|
| lower heating value, LHV (MJ/kg) | 19.34 |
| air composition (vol %) | 79 vol % $N_2$ and 21 vol % $O_2$ |
| rapeseed methyl ester (RME) | methyl oleate, $C_{19}H_{36}O_2$ |
| oxygen carrier | LD slag |

| LD slag composition (%, w/w) | $Fe_2O_3$ | MnO | $SiO_2$ | CaO | MgO | $Al_2O_3$ | $TiO_2$ | $K_2O$ |
|---|---|---|---|---|---|---|---|---|
| | 28.8 | 3.3 | 14.1 | 42.0 | 9.1 | 1.2 | 1.3 | 0.09 |

| Process Conditions (Cases CG and HG) | |
|---|---|
| **CLG** | |
| fuel inlet temperature (°C) | 25 |
| gasifier steam inlet temperature (°C) | 500 |
| air inlet temperature (°C) | 450 |
| CLG operating pressure (bar) | 1 bar (case CG) and 10 bar (case HG) |
| steam/biomass ratio, S/B (kg/kg$_{db}$) | 0.6−1.2 |
| char (CISOLID) conversion assumed in the FR submodels (%) | 100 |
| degree of oxidation in the AR (%) | 100 |
| **Gas Cleaning and Conditioning** | |
| tar removal separation efficiency | 100% $C_6H_5OH$, 100% $C_7H_8$, and 100% $C_{10}H_8$ |
| RME consumption in the tar scrubber unit[45] | 0.03 $MW_{RME}/MW_{fuel}$ |
| amine scrubber separation efficiency[46,47] | 96% $H_2S$, 62% $CO_2$, 100% $NH_3$, 0.0738% $CH_4$, 0.0581% CO, and 0% $H_2O$ |
| HT-WGS (case CG) | $H_2O$/CO = 3, 350 °C, and 30 bar |
| HT-WGS (case HG) | $H_2O$/CO = 3, 350 °C, and 10 bar |
| **FTS** | |
| FT reactor temperature | 220 °C and 30 bar |
| CO conversion, $X_{CO}$ (%) | 70 |
| autothermal reformer | 1000 °C and 30 bar |
| Rectisol separation efficiency[36] | 96.8% $CO_2$, 100% $H_2S$, and 100% $NH_3$ |

intermediate pressure of 10 bar to compensate for pressure drops in the downstream reactors and favor lower catalyst requirements. In this work, a selective Rectisol[36] unit with its estimated separation efficiencies is assumed for deep cleaning of syngas and $CO_2$ capture prior to the FT reactor. The simple schematic of the two process configurations modeled in this work is shown in Figure 2.

The main basis for the CLG model was experiments performed with LD slag, a byproduct stream from the steel industry. Similar materials are available from other industries, for instance, iron-rich sintered copper smelter slag, which has been investigated experimentally by Wang et al.[37] This has been used as the primary OC in this work mainly as a result of its inherent benefits associated with limited oxygen transport capacity, availability, agglomeration, and expected low cost associated with material preparation and handling confirmed by CLG experiments[11,17] and oxygen-carrier-aided combustion experiments[38,39] at different scales. In addition to this, LD slag has a high calcium content that could favor WGS activity in the FR.[11] It is estimated to have a maximum oxygen transport capacity (OTC) of 1.12% by weight.[40,41] Condori et al.[18] also reported an OTC of 1.2% for used LD slag after 60 h of operation, and 1.8% for unused or fresh LD slag. In cases CG and HG, the active species assumed in LD slag is hematite that is restricted to $Fe_2O_3$/$Fe_3O_4$ oxide couple, owing to the

thermodynamic limitation on its reduction.[42−44] Both cases are described in more detail in the following section.

## 4. PROCESS AND MODELING DESCRIPTION

The integrated CLG−FT process model description is divided into three sections, namely, CLG, syngas cleaning, and FTS. Steady-state process models of CLG and gas cleaning are developed using Aspen Plus version 10 software. A FTS model developed by Pondini and Ebert[33] is integrated with the developed CLG and syngas cleaning models to evaluate the overall plant performance. A summary of feed streams and assumptions in the three sections of the CLG−FT process chain are listed in Table 5.

**4.1. CLG.** The Peng−Robinson equation of state with Boston−Mathias modifications (PR-BM) thermodynamic property method is used in the model that has been commonly used for developing gasification-based process models.[48,49] Biomass is defined as a non-conventional (NC) component with its ultimate and proximate analysis data, and the HCOALGEN and DCOALIGT methods[50] are used to calculate the enthalpy of biomass and the densities of biomass and ash, respectively. In both cases, the biomass is assumed to have undergone drying before being fed into the gasifier. In addition to the assumptions listed in Table 5, other modeling assumptions are summarized as follows, and their influence on the whole process is discussed in the subsequent text and
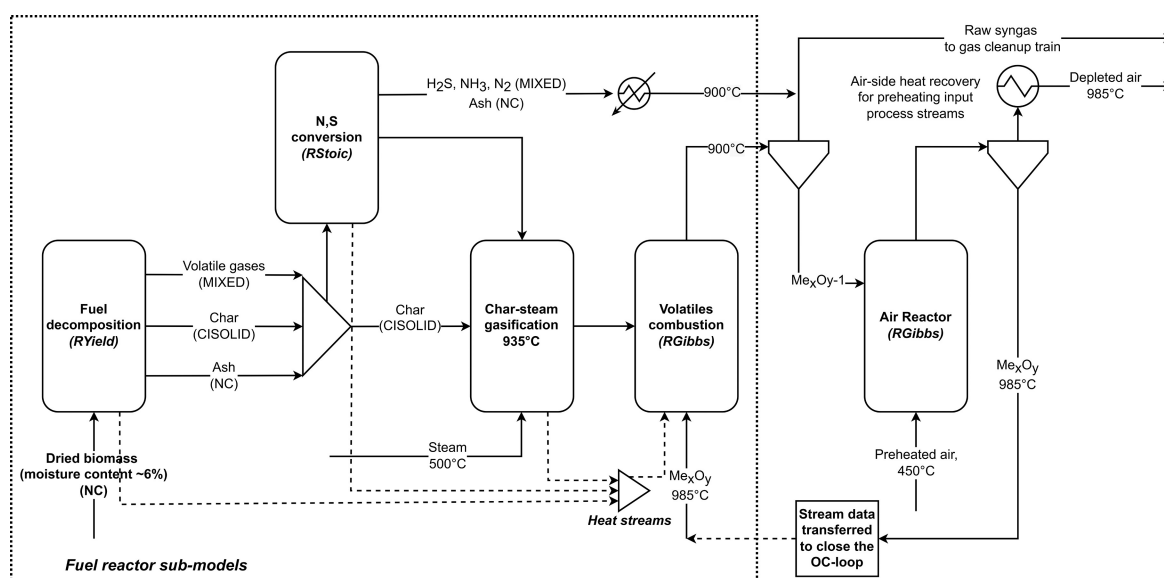
**Figure 3.** Process schematic of the CLG model, with the FR modeled using four submodels.

**Table 6. Description of Main Unit Operators Used in the CLG Model for Cases CG and HG**

| main unit | submodel | unit operator | description |
|---|---|---|---|
| FR | fuel decomposition | RYield | biomass is defined as a NC component, assumed to instantaneously decompose to its constituent elements: ash (NC), char (CISOLID), and volatile gases (MIXED) as per eq R7 |
| | N and S conversion | RStoic | 100% sulfur conversion to $H_2S$ and 60% fuel-bound N converted to $NH_3$ |
| | char−steam gasification | RStoic | stoichiometric reaction defined by a mechanism factor; $\alpha = 1.1$ as per eq R8; S/$B_{db}$ ratio = 1; 935 °C |
| | volatile combustion | RGibbs | adiabatic reactor, with specified expected products at the outlet; expected gas−solid reactions (eqs R15−R19) |
| AR | OC oxidation | RStoic | adiabatic reactor; calculator adjusts OC circulation rates to achieve an AR outlet temperature of 985 °C; expected oxidation reaction (eq R22) |

Section 5: (1) No reactor heat losses are considered. (2) Pressure drop in the CLG model is not considered. (3) Instantaneous devolatilization of biomass is assumed in the FR submodels. (4) Complete conversion of char in the FR is assumed; thus, there is no char leakage to the AR. (5) Complete oxidation of the OC in the AR. (6) Fuel-bound sulfur completely converts to hydrogen sulfide; fuel-bound nitrogen converts to mostly $NH_3$; and the rest converts to $N_2$. (7) $Fe_2O_3$/$Fe_3O_4$ are assumed to be the active species in the OC.

Further, corrosive elements, such as chlorine, are not considered. Char is assumed to be 100% carbon graphite and is defined as a solid (CISOLID) component, and ash is defined as a NC component in the model. LD slag that is fed to the system with its constituent elements, as shown in Table 5, is also defined as solid components in the model. The process flow diagram of the CLG section is shown in Figure 3, and the unit operators used in the model are listed in Table 6. As the reactions taking place in the FR are rather complex, the FR was modeled with four submodels, namely, fuel decomposition, char−steam gasification, fuel-nitrogen and sulphur conversion, and finally, volatile combustion through gas−solid reactions in the FR, shown in Figure 3.

*4.1.1. Fuel Decomposition.* In the process model, biomass defined as NC, with its ultimate and proximate analysis data, is fed to the fuel decomposition (RYield) block in Figure 3, which simulates the decomposition of biomass into its constituent elements on a mass basis, and the yield distribution is given as input in this block that is calculated and set by
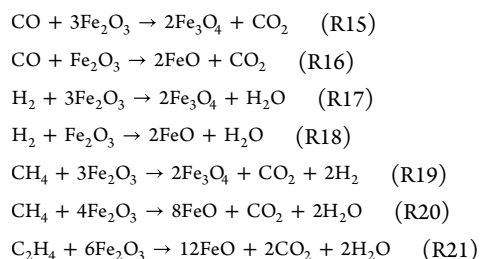
Fortran statements written in a calculator block. Biomass is assumed to have undergone instantaneous devolatilization, and it decomposes into volatile gases (MIXED substream), ash (NC), and char (CISOLID), as depicted in Figure 3. Heat streams are used to account for the endothermic steps in the FR submodels and are integrated into the volatiles combustion (RGibbs) submodel, shown as dashed lines in Figure 3. The other conventional components (H, N, O, and S) and ash are directed to the N and S conversion (RStoic) block, and the char component is directed to the char−steam gasification (RStoic) block, where it undergoes reactions shown in Table 3 (eq R8).

*4.1.2. Nitrogen and Sulfur Conversion.* This block assumes the complete conversion of sulfur to hydrogen sulfide, while fuel-bound nitrogen predominantly becomes ammonia. However, some nitrogen oxides are also expected as a result of the higher oxidizing environment compared to conventional gasification systems. It is well-known that $NH_3$ can become oxidized to $NO_x$ by some common OCs.[51,52] In this (RStoic) block, 60% of fuel-bound nitrogen is assumed to become converted to ammonia, and the rest remains as $N_2$. The conventional gases are separated from the gas impurities and directed back to the char−steam gasification block, while ash and gas contaminants are heated and mixed back with product gases from the final submodel of the FR, i.e., volatile combustion (RGibbs) block. This is performed to obtain raw syngas, including their contaminants, as the input stream for the subsequent gas cleaning section.

*4.1.3. Char–Steam Gasification.* This char–steam gasification block, shown in Figure 3, is an isothermal stoichiometric reactor operating at 935 °C and ambient pressure, i.e., the operation conditions of the FR. Char undergoes gasification with steam, as per the combined equation of char–steam gasification and water–gas shift reaction, as shown in eq R8 in Table 3, where a factor ($\alpha$) of 1.1 is assumed as the FR operates above 900 °C. Methane and tar (phenol, toluene, and naphthalene) formation reactions are also specified in the block. Pissot et al.[11] evaluated CLG using LD slag with varying fractions of sand on a high-volatile fuel, where the tar yield of roughly 30 g/kg$_{daf}$ including benzene, toluene, and xylene (BTX), was estimated. Larsson et al.[53] investigated ilmenite, as the OC, in a DFB gasifier that indicated lowered tar yields as a result of the presence of a higher oxidizing environment and its catalytic effect on tars; however, an increasing trend of heavier tars was also noticed. On the basis of these findings of tar formation in CLG, a calculator block is used to simulate tar formation with the expected yield, which mainly consisted of phenol ($C_6H_6O$), naphthalene ($C_{10}H_8$), and toluene ($C_7H_8$). Heat streams are used to integrate the char–steam gasification block with the adiabatic volatile combustion (RGibbs) block, shown as a dashed line in Figure 3, to account for the heat demand in this submodel. This is performed to simulate the heat balance over the FR. Although complete conversion of char is assumed in the overall CLG model, the char conversion is dependent upon the S/B$_{db}$ ratio or the steam fed to the char–steam gasification (RStoic) block in the CLG model. In both cases of the CLG model, it is assumed that there is no carbon leakage into the AR (RStoic) block, owing to high carbon conversion achieved in the FR and low carbon leakage to the AR (<1%) expected in larger CLG plants.[17]

*4.1.4. Volatile Combustion.* A RGibbs block is used to model the gas–solid reaction between the volatile gases and the OCs. In case CG, it is assumed that only $Fe_2O_3$ in the LD slag provides lattice oxygen for the gasification reactions, and the corresponding gas–solid reactions that are expected in the FR are listed in Table 7.

**Table 7. Gas–Solid Reactions Expected in the Volatile Combustion Submodel**

$$CO + 3Fe_2O_3 \rightarrow 2Fe_3O_4 + CO_2 \quad (R15)$$

$$CO + Fe_2O_3 \rightarrow 2FeO + CO_2 \quad (R16)$$

$$H_2 + 3Fe_2O_3 \rightarrow 2Fe_3O_4 + H_2O \quad (R17)$$

$$H_2 + Fe_2O_3 \rightarrow 2FeO + H_2O \quad (R18)$$

$$CH_4 + 3Fe_2O_3 \rightarrow 2Fe_3O_4 + CO_2 + 2H_2 \quad (R19)$$

$$CH_4 + 4Fe_2O_3 \rightarrow 8FeO + CO_2 + 2H_2O \quad (R20)$$

$$C_2H_4 + 6Fe_2O_3 \rightarrow 12FeO + 2CO_2 + 2H_2O \quad (R21)$$

It is important to note here that, in both cases, as the redox reactions are thermodynamically limited to oxide couples of $Fe_3O_4$/$FeO$ and $FeO$/$Fe$,[42−44] the expected metal oxide products are specified as the $Fe_2O_3$/$Fe_3O_4$ oxide couple in the RGibbs reactor. Gas–solid reactions (eqs R20 and R21) are thus not considered in this reactor as no FeO is expected in the product stream. The pseudo-equilibrium approach described by Arvidsson et al.[54] for a biomass-based syngas production plant is adopted in this work to avoid the complete decomposition of methane and tar components in the Gibbs

reactor. Calculator blocks are used to set the expected fractions of $CH_4$ and tar components from the FR. The gasification gases and reduced OC from the FR are separated in a SSplit block that simulates the cyclone after the FR, where the exiting raw syngas is mixed back with the heated gas contaminant stream from the N and S conversion block and the reduced OCs are directed to the AR block, shown in Figure 3.

*4.1.5. AR.* The AR is an adiabatic stoichiometric reactor, where it is assumed that 100% of the reduced OC from the FR oxidizes with air. Table 8 shows the expected oxidation

**Table 8. Oxidation Reactions of OC in the AR**

| reaction | | $\Delta H$ (kJ/mol) |
|---|---|---|
| $4Fe_3O_4 + O_2 \rightarrow 6Fe_2O_3$ | (R22) | −479 |
| $4FeO + O_2 \rightarrow 2Fe_2O_3$ | (R23) | −560.66 |

reactions (eqs R22 and R23) in the AR. These reactions are typically rapid; thus, the residence times in this reactor are expected to be low. In this case, however, only oxidation of magnetite ($Fe_3O_4$) is considered, as no FeO compounds are expected at the outlet of the volatile combustion submodel as a result of the restricted oxide couple specification in the Gibbs reactor.

A design specification block is used to set the air required for complete oxidation of incoming reduced OC to the AR block. No carbon leakage to the AR is assumed in the model. The air is assumed to be heated to roughly 450 °C, recovering the heat from oxygen-depleted air from the AR outlet. The resulting oxygen-depleted air and solids are separated in a cyclone, using a SSplit block in the model.

*4.1.6. OC Circulation.* OTC is defined as the maximum oxygen that can be transferred between the AR and FR for a given mass flow of circulating OC particles[55] and calculated as shown in eq 8 in Table 10. On the basis of various factors during operation, it is expected that the maximum OTC of the OC is not achieved. The mass flow rate of the OC feed stream must be controlled to achieve an autothermal operation. Thus, the OC feed stream to the volatile combustion (RGibbs) stage is defined with the mass compositions of fully oxidized OC with a temperature of 985 °C. The mass flow rate of this feed stream is set by a calculator block to match the stream composition and conditions, with the returning oxidized OC stream from the AR (RStoic) block. This OC recirculation is shown as a dashed line in Figure 3.

**4.2. Syngas Cleaning and Conditioning.** The process modeling and configuration of the cold-gas and hot-gas cleanup train used in cases CG and HG, respectively, are discussed in this section.

*4.2.1. Cold-Gas Cleanup (Case CG).* In case CG, the gas cleaning stage has been modeled as a CGCU train with conventional gas cleaning technologies, as shown in Figure 4. Here, the gas cleanup train is adapted from Arvidsson et al.,[54] where a similar gas cleaning train was suggested for a bio-to-SNG production process. The main unit operators used in this section are described in Table 9.

In case CG, the raw syngas from the FR is cooled to 210 °C, where the heat is recovered, which is followed by ash and solids removal, modeled using a separation (Sep) block. RME-based tar scrubbers are modeled here, using the data from the GoBiGas plant, where a RME consumption of 0.03−0.035 MW$_{RME}$/MW$_{fuel}$ was reported.[45] This tar-free syngas is then
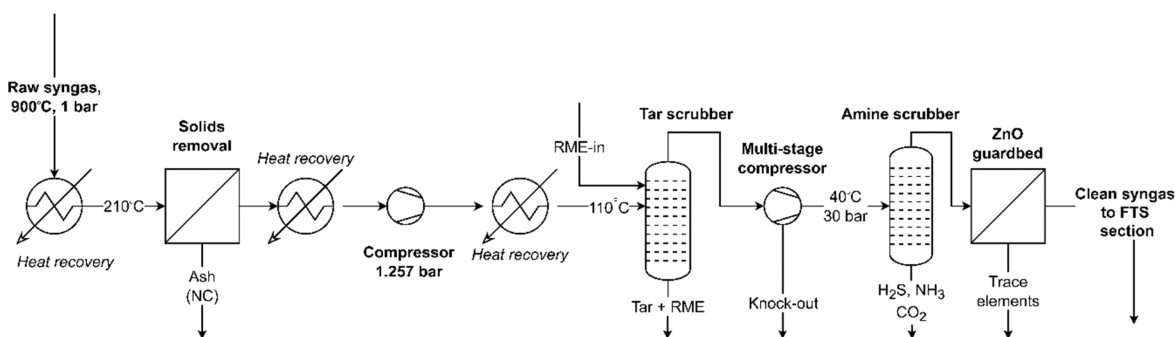
**Figure 4.** Process flow diagram of the syngas cleaning section depicting the CGCU train in case CG.

**Table 9. Main Operators Used in the Gas Cleaning Stage in Case CG (CGCU)**

| main unit | unit operator | $T_{out}$ (°C) | $\Delta p$ (bar) | description |
|---|---|---|---|---|
| solids removal | SSplit | 210 | −0.2 | slag stream, NC split fraction set as 1 |
| compressor | Compr | 209 | 0.425 | set to compensate for the pressure drop in the RME scrubber |
| multi-stage compressor | MCompr | 40 | −0.2 | three stages, cooler outlet temperature: 80, 80, and 40 °C, no dP in coolers |
| tar scrubber | Sep | 30 | 0 | RME-based scrubber, 100% tar and RME removal, split fractions set as 1 |
| amine-based scrubber | Sep | 40 | 30 | MDEA-S absorber, split fractions set based on separation efficiencies (%)[46,47] |
| trace removal | Sep | 40 | −0.2 | 100% S removal assumed |
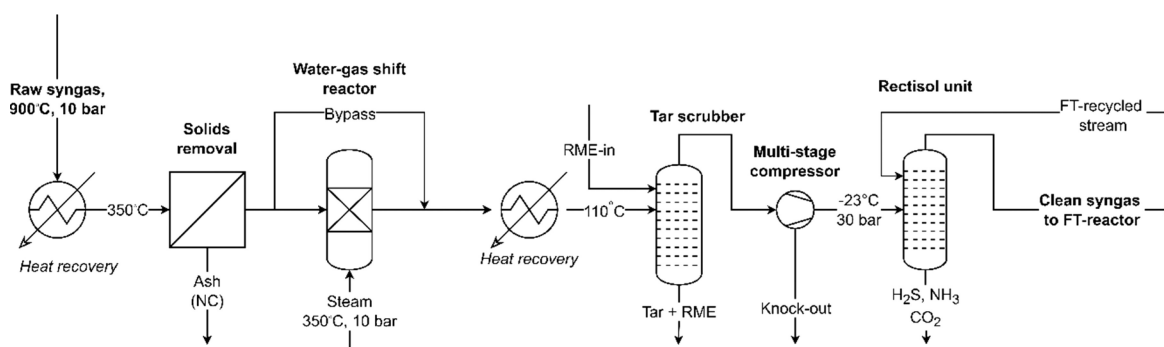


**Figure 5.** Process flow diagram of the HGCU train modeled in case HG.

cooled and compressed in a multi-stage compressor block prior to a conventional amine scrubber unit, where separation efficiencies from the literature are given as input to the separation block. This block separates around 62% of incoming $CO_2$ that is available for storage or utilization. The syngas is further cleaned and removed of trace elements using a ZnO-based guard bed to obtain a clean syngas, free of impurities, that is obtained at low temperatures and high pressures at the end of this CGCU train, and this clean syngas stream requires heating to temperatures desired in the downstream water−gas shift reactor in the FTS model, described in Section 2.3.

*4.2.2. Hot-Gas Cleanup Train (Case HG).* The CGCU train in case CG, with the CLG process operating at ambient pressures, was modified to a HGCU train in case HG with the CLG model operating at an intermediate pressure of 10 bar. The higher operating pressure at the gasification side favors lower catalyst requirements and compensates for pressure drops in the catalytic reactors and scrubbers downstream. This process configuration starts with solids removal, followed by a sulfur-resistant water−gas shift reactor and tar scrubber, followed by the Rectisol unit in the FTS section. In this HGCU configuration, the AGR unit for $CO_2$ capture is reduced to one unit compared to the two capture units, namely, the amine scrubber and Rectisol unit in the CGCU train. On the basis of the experiments with commercially

acquired Fe−Cr catalysts, it was reported that a HT-WGS reactor could be operated with tar-rich product gas that has undergone filtration for solids removal.[56,57] Therefore, the HT-WGS is placed before the tar scrubber and the Rectisol unit, as shown in Figure 5. An iron−chromium-based high-temperature (HT-WGS) reactor is assumed and modeled using an equilibrium-based (RGibbs) reactor. As high $H_2/CO$ ratios are generally expected from a CLG compared to the IG process, the HT-WGS reactor is modeled with a bypass stream, because a relatively lower amount of gas conditioning is required to reach the desired $H_2/CO$ ratio (∼2.0−2.15) for the FTS process. The HT-WGS reactor typically operates at 350−550 °C, with the operating pressure dependent upon the upstream process.[57,58] In addition to this, the WGS reaction is favorable at lower temperatures. Thus, the raw syngas from the FR is cooled to the lower range of 350 °C prior to the HT-WGS reactor. To avoid methanation, coking, and carbon deposition on the catalyst surface, the steam/carbon ratios on a mass basis are typically between 2.8 and 4.2.[59] The chosen operating conditions regarding the WGS reactor in this section are listed in Table 5. The process flow diagram of the HGCU train modeled is shown in Figure 5, and the Rectisol unit shown in this figure is discussed in more detail in the following section.

**4.3. FTS.** In this work, a cobalt-based LTFT synthesis model is used for the downstream fuel synthesis stage, adapted
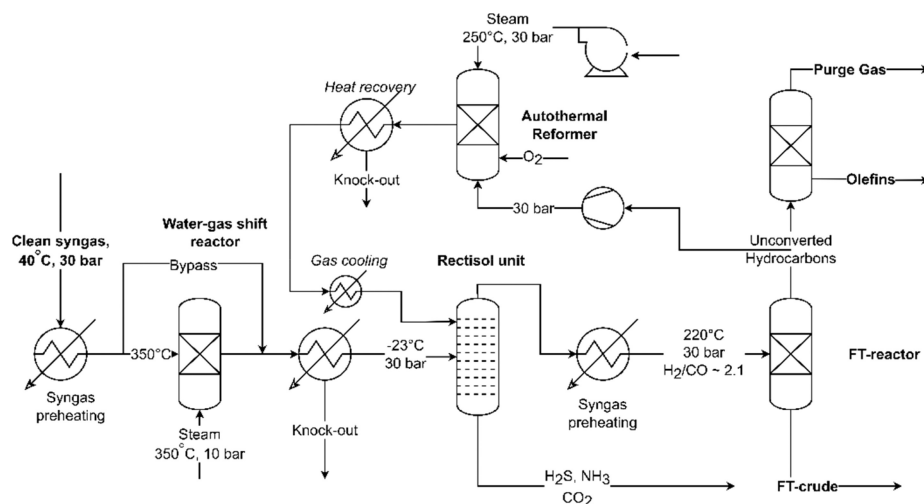
**Figure 6.** Simplified process flow diagram of the FTS process integrated with case CG, following the gas cleaning (CGCU) section shown in Figure 4.

from previous works of Pondini and Ebert.[33] The process flow diagram of the LTFT synthesis plant is shown in Figure 6. Process conditions favoring an increased heavier hydrocarbon yield from the FTS process were chosen in the FT reactor used in this work. The main unit operators and operating conditions of the FTS model are listed in Table S1 of the Supporting Information.

Figure 6 shows a simplified flow diagram of the FTS section in case CG. A simplified description of the FTS process model in case CG is as follows: A high-temperature WGS reactor is used prior to the FT reactor to condition the syngas to a desired $H_2/CO$ ratio of 2.05–2.15 for the FTS process. The incoming clean syngas (at 40 °C and 30 bar pressure) is heated prior to the HT-WGS. Steam is supplied to the WGS reactor at 350 °C and 30 bar pressure, and the amount of steam required in the WGS reactor is set by a calculator block by defining a $H_2O/CO$ ratio of 3.0 at the WGS inlet. As a high $H_2/CO$ ratio is expected from the CLG process, only a fraction of the clean syngas needs to be reformed in the WGS reactor; thus, the clean syngas stream is split using a SSplit block, and the rest of the stream is bypassed. In case HG, this is completely bypassed as a result of the hot-gas cleanup train. Thus, economic gain is expected associated with gas conditioning in the WGS reactor in both cases, and this is discussed in Section 6. The split fraction in the SSplit block is adjusted in a calculator block to achieve a $H_2/CO$ ratio of 2 prior to the Rectisol unit, needed to remove $CO_2$ from the gas after the WGS reactor.

The Rectisol unit operates at sub-ambient temperatures; thus, the shifted clean syngas is cooled and flashed prior to the Rectisol unit and subsequently compressed to pressures required in the FT reactor. For the Rectisol unit in this work, a separator (Sep) block has been used with the expected separation efficiency of $CO_2$ and other gas impurities, such as $H_2S$ and $NH_3$, specified in this block. Commercial Rectisol units have $CO_2$ removal efficiency constrained to 60%, owing to energy consumption constraints.[36] In contrast to this, a conceptual $CO_2$ capture process based on Rectisol modeled by Yang et al.[36] estimated $CO_2$ removal efficiencies close to 98.6%. In addition to this, the energy consumption per unit of $CO_2$ captured in this process (~25.8 kJ/mol) was estimated to be one-fifth of that of a conventional Rectisol process. In this work, separation efficiencies, feed stream cooling, and specific

energy consumption are assumed on the basis of this suggested process.[36]

The FT reactor is modeled as a stoichiometric (RStoic) reactor, with a calculator block that predicts hydrocarbon distribution based on probability distribution models. More information on the modeling assumptions and other parameters used in this block can be found elsewhere.[33] Two separate streams are obtained from the FT reactor after flashing: the heavier fraction of liquid hydrocarbons and the unconverted hydrocarbon gases. The heavier hydrocarbons, i.e., FT crude, are the final product obtained from this process. The majority of the unconverted gases from the FT reactor, which mainly consists of $H_2$, CO, and $CH_4$, are recycled in the FTS section with a shorter recycle loop, and the rest, roughly 10% of these gases, are purged to avoid buildup of inert components in the FT reactor. Olefins are recovered from these purged gases, and the rest of the gaseous vapors are recycled to the ATR. The ATR converts methane from the gasification stage as well as the FT reactor. The unconverted hydrocarbon gases are reformed in the ATR at 1000 °C with steam and oxygen fed to the reactor. A calculator sets the required oxygen input to combust part of the lighter hydrocarbons in the recycled stream to maintain the ATR outlet temperature at 1000 °C. In case HG, the clean syngas from the Rectisol unit, shown in Figure 5, is directly fed to the FT reactor in this section, and the short recycle loop of the unconverted hydrocarbon gases to the ATR nevertheless remains unchanged. This work does not include the product upgrading stage as this is a mature technology in the oil and gas industry. Different process configurations and integration aspects of the product upgradation of FT crude produced from a FTS at an oil refinery can be found elsewhere.[60]

## 5. RESULTS AND DISCUSSION

**5.1. Model Validation.** The CLG model operating at ambient pressures has been validated with experimental investigations performed at Chalmers by Moldenhauer et al.[17] on CLG with LD slag as the OC. The CLG experiments were performed in a 10 kW pilot unit with FR temperatures around 965–985 °C with three different fuels: black pellets, wood char, and wood pellets. The measured data with wood pellets were considered for validating the developed model, as
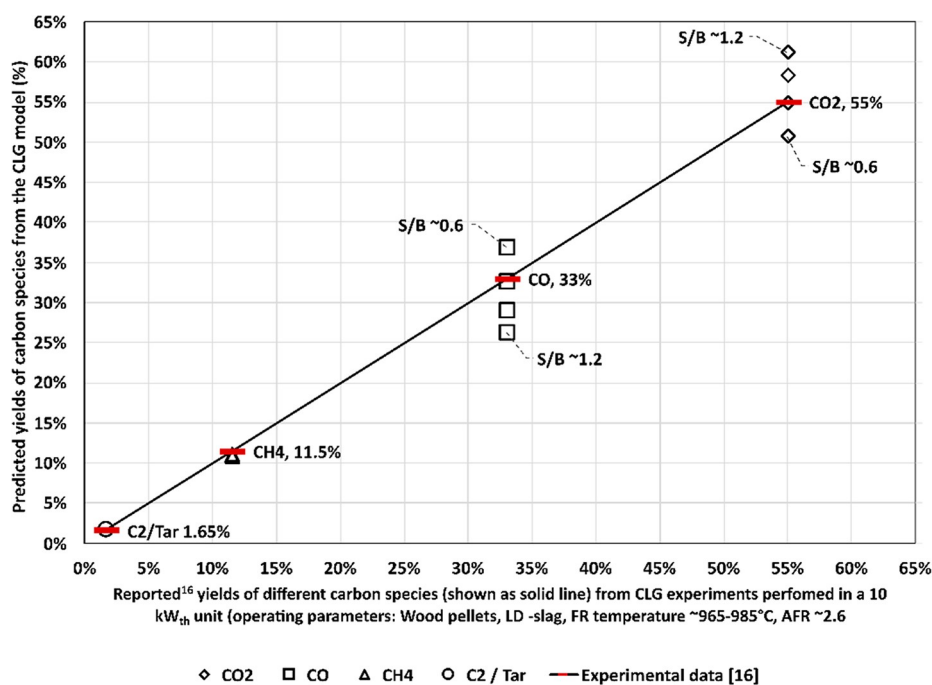
**Figure 7.** Comparison of the predicted fractions of carbon species from the FR in the CLG model to the reported carbon fractions in the 10 kW$_{th}$ pilot unit.
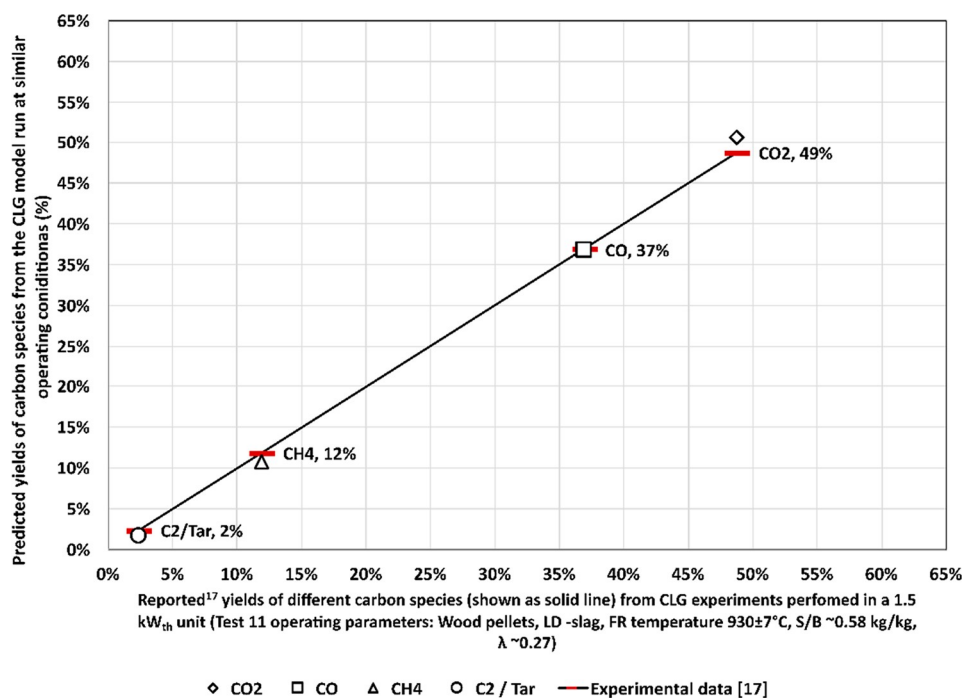


**Figure 8.** Comparison of experimental fractions of carbon species from tests performed at 930 °C, S/B ratio of 0.58, and $\lambda$ of 0.27[18] to the carbon fractions predicted in the CLG model at a FR temperature of 935 °C, S/B ratio of 0.6, and $\lambda$ of 0.30.

its fuel composition is comparable to the forest residue feedstock used in the CLG model. Three data points of yields of different carbon species ($CO_2$, CO, $CH_4$, and $C_2$ species) were reported[17] with varying air/fuel ratios for the case with wood pellets. The experiments with wood pellets were performed with an air/fuel ratio ranging from 2.9 to 7.0. Here, the reported yields of carbon species with AFR of ∼2.9 are chosen for comparison to the developed CLG model. There are two reasons for selecting this specific operating point. First, the pilot unit operates with a higher AFR as a result of designing the unit for operational flexibility.[17] Further, it can be motivated by the assumption made in the CLG model that no excess air is supplied to the AR block and that there is no char leakage to the AR. As there was no information regarding the steam/biomass (S/B) ratio used during these tests, the model-predicted fractions of carbon species, with varying S/B$_{db}$ ratios ranging from 0.6 to 1.2, were compared to available experimental data, shown in Figure 7.

In Figure 7, reported carbon yields are plotted as a solid line, with the yields of different carbon species[17] shown with red markers. Here, the carbon yields predicted from the CLG models with varying S/B ratios are plotted as black scattered points for comparison to the experimental data. The tar and methane fractions predicted from the model have little variation from the experimental data as a result of using Fortran statements to calibrate the FR submodels to incorporate the thermodynamic equilibrium deviations associated with methane and tar formation. As no $C_2$ species were specified in the model, the lumped tar components are shown along with the $C_2$ species yield reported in the 10 kW unit tests. The average absolute deviation (%) was estimated to be the lowest (<2.5%) for the predicted carbon yields from the CLG model, with a S/B ratio of 0.8, when compared to the experimental data, shown in Figure 7. However, it is important to note that there are minor differences in the operational conditions/parameters during the experimental tests, for example, higher AFR ratios used in the pilot unit, owing to flexibility reasons,[17] and slightly higher temperatures in the unit compared to the temperatures taken in the model, which could result in slight variations in predicted carbon species fractions. In case CG, with the restriction on iron oxide reduction to the $Fe_2O_3/Fe_3O_4$ oxide couple, the model predicts a maximum oxygen transport capacity of 0.963%, and this is comparable to the maximum oxygen transport capacity of 1.12% for LD slag reported in the literature.[40]

Further, the model is validated with a more recent experimental study on CLG of industrial wood pellets (IWP) with LD slag as the OC in a 1.5 $kW_{th}$ unit performed by Condori et al.[18] Here, the tests were performed for different gasification agents (steam and $CO_2$), wide-ranging S/B ratios, and oxygen/fuel ratios ($\lambda$) to investigate the effect on raw gas compositions. The gas compositions reported for the closest operational conditions (test 11[18] performed with a S/B ratio of 0.58 and $\lambda$ of 0.27) with the modeled CLG model are considered for model validation. The reported gas compositions are translated to yields of carbon species that are shown as red markers along the solid line in Figure 8. The predicted fractions of carbon species in the raw syngas from the CLG model run at a S/B ratio of 0.6 with $\lambda$ of 0.30 are plotted against the reported experimental data.[18]

As the syngas compositions reported in the literature with CLG experiments are both limited and performed thus far in smaller units (<25 $kW_{th}$[10]), another metric to further compare the model results to larger pilot units is the ratio of initial OC circulated to fuel input (kg of OC/$MW_{th}$). Here, the 1 $MW_{th}$ CLC pilot plant in Technischen Universität Darmstadt (TU Darmstadt)[61] is used as the best reference, where the CLC unit was modified and operated for CLG experiments with biomass.[61] This pilot plant is a 1 $MW_{th}$ unit with a total bed inventory of 1000 kg with 80 kg of bed material in the FR.[61] The reported solids circulation is around 7000−7500 kg/h at the FR outlet, corresponding to a ratio of 1.94−2.08 kg of OC/$MW_{th}$.[61] In the developed CLG model with an initial OC input of 207.84−227.16 kg/s in cases HG and CG, respectively, the estimated specific circulation flow is around 2.08−2.27 kg of OC/$MW_{th}$, which is in a reasonable range when compared to the larger 1 $MW_{th}$ pilot plant.

For case HG, the validated CLG model is operated at an intermediate pressure of 10 bar to evaluate the performance of the more technically ready CGCU train with the HGCU train. Detailed stream data of the CLG and the syngas cleaning

section for the two-gas cleaning trains are presented in Tables S3 and S4 of the the Supporting Information. The different cases described above were evaluated using the performance indicators listed in Table 10. In the CLG model, oxygen for the

**Table 10. Summary of Performance Indicators Used To Evaluate the Different Cases of the CLG Model**

| performance indicator | |
|---|---|
| C fraction of carbon species in the syngas | $f_{CO_2} = \dfrac{n_{CO_2,sg}}{n_{CO_2,sg} + n_{CO,sg} + \sum_x (x n_{C_nH_m,sg})}$ (1) |
| | $f_{CO} = \dfrac{n_{CO,sg}}{n_{CO_2,sg} + n_{CO,sg} + \sum_x (x n_{C_nH_m,sg})}$ (2) |
| | $f_{CH_4} = \dfrac{n_{CH_4,sg}}{n_{CO_2,sg} + n_{CO,sg} + \sum_x (x n_{C_nH_m,sg})}$ (3) |
| | $f_{CT} = \dfrac{n_{CT,sg}}{n_{CO_2,sg} + n_{CO,sg} + \sum_x (x n_{C_nH_m,sg})}$ (4) |
| air/fuel ratio (AFR) | $AFR = \dfrac{n_{O_2,AR_{in}}}{n_{O_2,comb}}$ (5) |
| steam/biomass ratio, S/B (kg/kg$_{db}$) | $S/B = \dfrac{\dot{m}_{steam}}{\dot{m}_{biomass}}$ (6) |
| lower heating value of syngas (MJ/Nm$^3$)[62] | $LHV_{sg} = 10.79 V_{H_2} + 12.63 V_{CO} + 35.82 V_{CH_4}$ (7) |
| oxygen transport capacity (%) | $OTC = \dfrac{\dot{m}_{ox} - \dot{m}_{red}}{\dot{m}_{ox}}$ (8) |
| cold gas efficiency (%) | $CGE = \dfrac{LHV_{sg} G_v}{LHV_{fuel,db} m_{fuel}}$ (9) |
| chemical efficiency (%) | $\eta_{ch} = \dfrac{HHV_{product} \dot{m}_{product}}{(HHV_{biomass} \dot{m}_{biomass}) + Q_f}$ (10) |

gasification is provided partially by the reduction of the OCs in the FR, and subsequently, complete oxidation of OC particles is assumed in the AR. Therefore, the amount of oxygen ($n_{O_2,AR_{in}}$) required to oxidize the reduced OC particles completely in the AR is taken as oxygen provided by the OCs. $O_2$-COMB property data in Aspen Plus is used to calculate stoichiometric oxygen required for complete combustion of the fuel stream into the FR.

The gasification performance is evaluated by the cold gas efficiency (CGE) calculated as the ratio between the energy content of the product syngas (LHV basis) to the energy content of biomass fuel input on a dry basis, as shown in eq 9, where the energy content of the syngas is calculated as per eq 7. Chemical efficiency, i.e., the conversion efficiency of biomass-to-FT crude, is calculated as the ratio of the total energy content of the FT crude produced (HHV basis) to the biomass fuel input to the CLG plant, including the RME consumption in the tar scrubber ($Q_f$), as shown in eq 10. In the following sections, sensitivity analyses were performed on the validated CLG model used in case CG.

**5.2. Effect of the S/B Ratio.** The syngas composition (vol %, dry basis) from the FR is shown in Figure 9, with varying S/B ratios (dry basis) for case CG. The hydrogen yield, as expected, tends to increase with the increase in steam fed to the system, while at the same time, $CO_2$ follows the same trend as hydrogen. Thus, this indicates an increased water−gas shift reaction at the expense of carbon monoxide. Pressurized operation of the CLG model in case HG has little effect on the
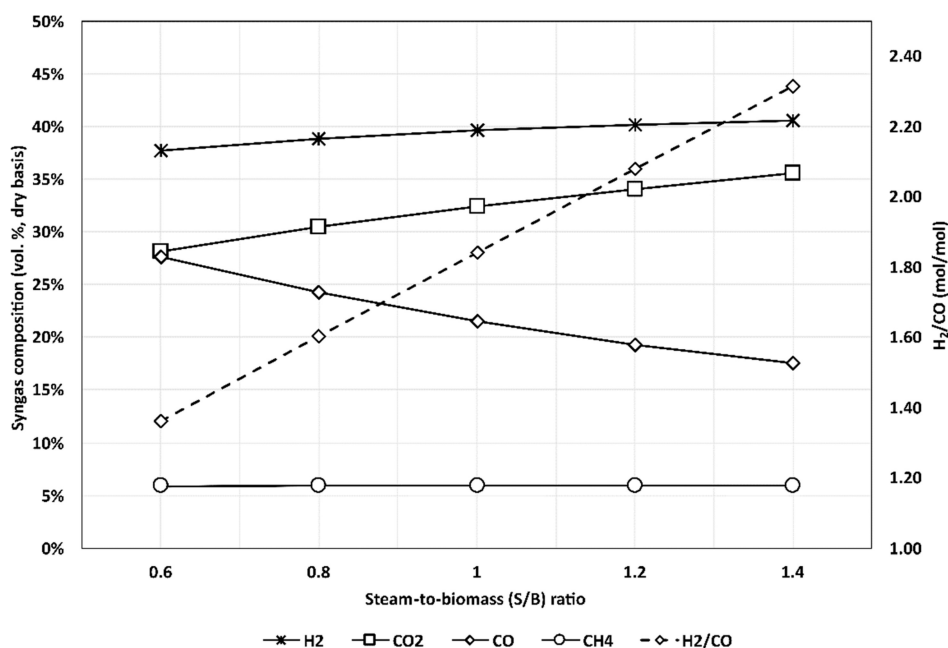
**Figure 9.** Effect of the S/B ratio on the dry syngas composition in case CG of the CLG model with the FR operating at 935 °C and 1 bar pressure.
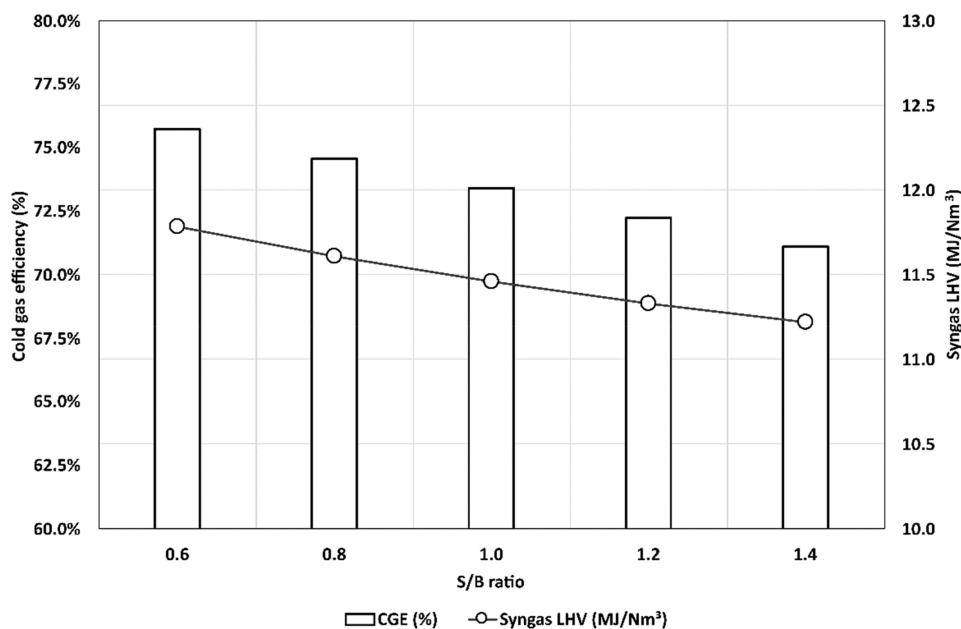


**Figure 10.** Effect of the $S/B_{db}$ ratio on CGE (%) of the process in case CG.

dry syngas composition for a fixed S/B ratio. The syngas compositions in different stages of the gas cleaning train for both cases CG and HG are listed in the stream data in Table S3 of the Supporting Information.

The effect of varying the S/B ratio on the CGE for case CG is shown in Figure 10, using eqs 7 and 9 listed in Table 10. It also shows the estimated lower heating value of the cleaned syngas produced from the CLG process, which ranged from 11.2 to 11.8 MJ/Nm³. The average LHV (dry basis) of the syngas was approximately 11.54 MJ/Nm³.

The model predicts a CGE (LHV basis) of roughly 73.0% for a S/B ratio equal to 1.0. The CGE tends to decrease with increasing the S/B ratio in the model. The decrease in CGE seen here in Figure 10 can be attributed to the increased WGS reaction in the FR. This can also be clearly seen in the syngas

compositions in Figure 9. Although the CLG model assumes 100% char conversion, it occurs in two submodels via char–steam gasification as per eq R8 in Table 3, followed by the expected gas–solid reactions (eqs R15–R19) in the Gibbs reactor. The carbon conversion in the two submodels of the FR is shown in Figure 11.

Clearly, carbon or char conversion tends to increase in the SG (RStoic) reactor with an increase in the $S/B_{db}$ ratio. The optimum steam required for the process cannot be ascertained solely based on Figure 11 as a result of the char conversion assumption in the model. From Figure 11, it can also be seen that complete conversion of char is not attained in the SG submodel, even with a S/B ratio as high as 1.4, and the remaining char completely decomposes in the subsequent volatile combustion (RGibbs) submodel of the FR. This
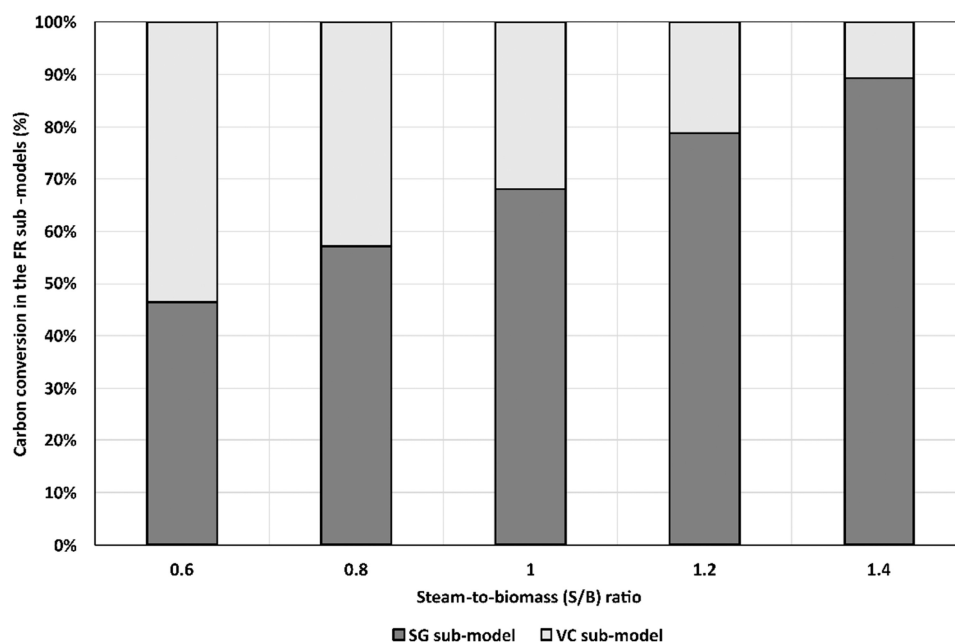
**Figure 11.** Effect of the S/B ratio on carbon conversion (%) in the FR submodels.
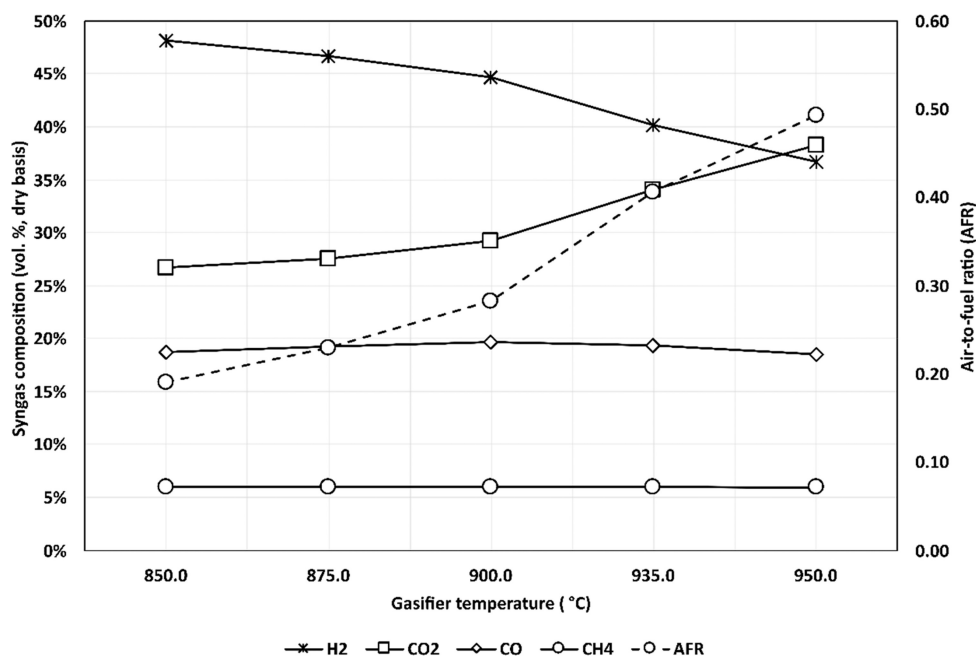


**Figure 12.** Raw syngas composition (vol %, dry basis) with a varying gasification temperature and the corresponding AFR.

decomposition in the Gibbs reactor is not calibrated as 100% char conversion is assumed in the model.

The CLG model was also tested with a biomass feed with a higher moisture content of 15%, which resulted in complete conversion of the char component in the SG model itself, with a relatively lower $S/B_{db}$ ratio of 1.0, as the biomass moisture largely remains as fluidization gases in the FR. This indicates a trade-off that exists between the syngas quality ($H_2/CO$ ratio) and the CGE, which is dependent upon the steam fed to the process. The model with a $S/B_{db}$ ratio lower than 1.0 estimates the $H_2/CO$ ratio at the FT reactor inlet at desired levels (>2.0), while the char conversion in the SG submodel is affected. Thus, the optimum $S/B_{db}$ ratio in the process is rather dependent upon achieving high char conversion in the FR,

where a moderate range of 1.0−1.2 is expected for a feed of dry biomass with 6% moisture content.

**5.3. Effect of the Gasification Temperature.** The effect of the gasification temperature (SG) on the syngas composition predicted by the CLG model in case CG is shown in Figure 12. The air/fuel ratio (AFR) in Figure 12 depicts the increase in OC circulation as a result of maintaining the autothermal operation between the two reactors. The increased OC circulation results in increased volatile combustion in the volatile combustion (RGibbs) submodel, which reflects an increase in the $CO_2$ concertation in the raw syngas at higher gasification temperatures.

**5.4. Effect of the Operating Pressure in the Gasification Stage.** The change in syngas composition and the
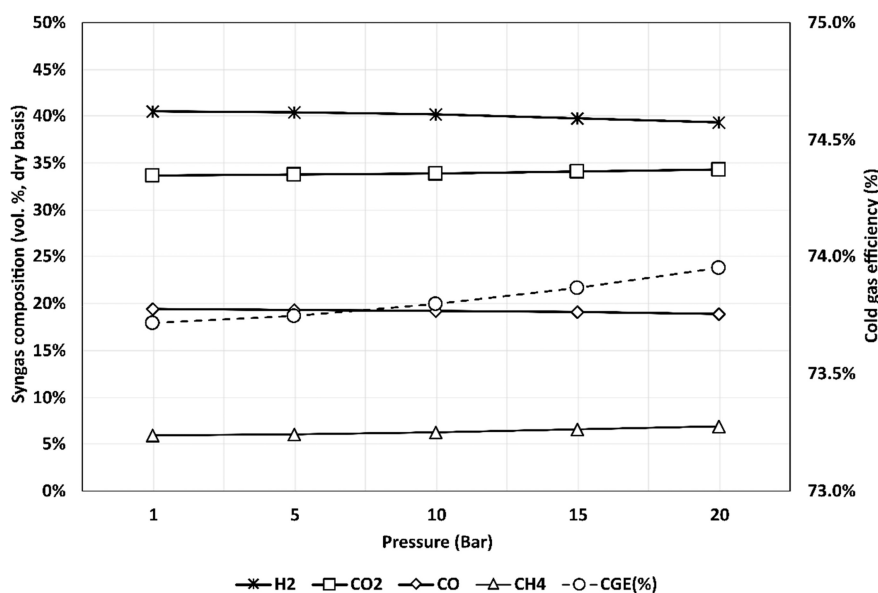
**Figure 13.** Effect of the pressure on the syngas composition and the corresponding CGE (%).
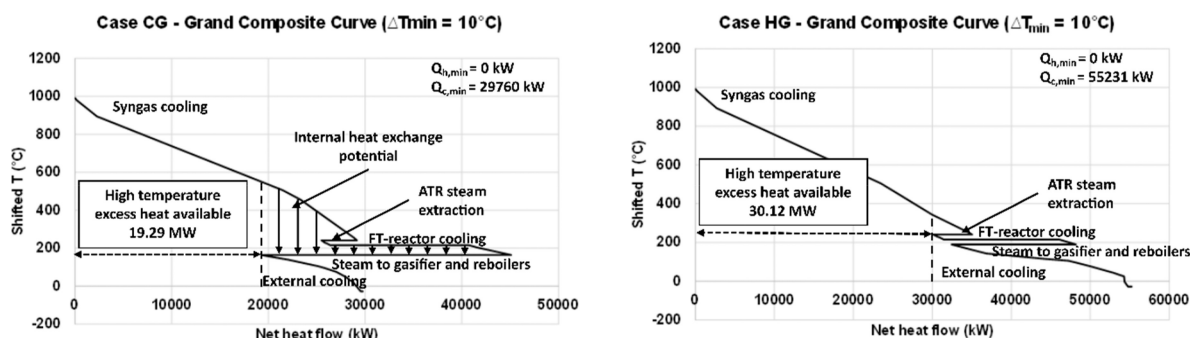


**Figure 14.** GCCs of cases CG and HG of the CLG−FT process.

corresponding CGE observed with varying gasification pressures from 1 to 20 bar is shown in Figure 13. In the CLG model, methane formation was calibrated using a calculator block based on available experimental data[17] at ambient pressures. For a higher operating pressure in the model, methane formation was extrapolated at equilibrium conditions and pre-processed in the calculator block, which is described in Section 4.1.4.

This sensitivity analysis was performed because operating the CLG section at an intermediate pressure could not only compensate for pressure drops in the scrubbers downstream but could also enable operating the WGS reactor at higher pressures. This could favor reaction rates in the shift reactor and, thereby, catalyst requirement in the reactor.[59] For a Fe−Cr-based catalyst, it is reported that the reaction rate increases with an increase in the pressure up to 21 bar, and thereafter, it plateaus.[59] In Figure 13, methane in the raw syngas increases with increasing pressure as a result of the calibration performed in the calculator block for methane formation at a higher pressure, at equilibrium conditions. As a result of increased methane formation at higher pressures, the energy content of the syngas from the FR increases slightly, and this can be seen in the corresponding biomass-to-syngas conversion efficiency, i.e., CGE, in Figure 13.

**5.5. Thermodynamic Evaluation.** The different process configurations in the gas cleaning stage of the two cases would influence the heating and cooling requirements in the overall process chain. Pinch analysis is performed to estimate the heat recovery potential from the two cases of the CLG−FT process using stream data from the simulation models. Pinch analysis is a systematic method to graphically estimate the heat recovery potential or targets for different energy processes.[63,64] Grand composite curves (GCCs) of cases CG and HG are shown in Figure 14, with a global minimum temperature difference ($\Delta T_{min}$) of 10 °C.

It can be seen from Figure 14 that high-grade heat is available for co-generation of heat and power at temperature levels above 200 °C. Above 200 °C, the potential for heat recovery is through syngas and oxygen-depleted air cooling. The other major source of heat is from the exothermic FT reactor operating at 220 °C. Heat sinks are primarily low-pressure (LP) steam generation for the gasifier and reboilers of the AGR units. The LP steam extraction level is 5 and 10 bar for cases CG and HG, respectively. In addition to this, an intermediate steam extraction pressure level of 30 bar, common in both cases, is chosen for the steam requirement in the ATR. The steam requirement in the Rectisol is assumed to be around 0.501 MJ/kmol of $CO_2$[36] and 3.3 MJ/kg of $CO_2$[65] for the amine scrubber in case CG. From the two cases, expectedly, more excess heat is available in case HG (30.12 MW) compared to case CG (19.29 MW). This is due to the requirement of an amine scrubber in the cold-gas cleanup train

of case CG. At temperatures below 200 °C, excess heat is available for feedwater heating. Further, at even lower temperature levels, external cooling utilities are required for sub-ambient cooling, mainly in the Rectisol unit.

**5.6. Performance of the Integrated Plant.** The fixed reference stream conditions considered in the two cases to evaluate the performance of the overall plant are listed in Table S2 of the Supporting Information. The syngas from the CLG process is upgraded to FT crude that contains long-chained hydrocarbons, namely, naphtha ($C_5$–$C_{11}$), FT diesel ($C_{12}$–$C_{19}$), and waxes (>$C_{20}$). Stream data of the FT crude and olefin output from the two cases are listed in Table S5 of the Supporting Information. The production distributions of the FT crude obtained from the two cases are listed in Table 11, along with other performance parameters, such as heat recovery potential, carbon capture capacity, and FT crude production efficiency.

**Table 11. Specific Process Characteristics for the Two Cases of the Integrated CLG−FT Model**

| process characteristic | | unit | case CG | case HG |
|---|---|---|---|---|
| minimum heating requirement | | MW$_{heat}$ | 0 | 0 |
| minimum cooling requirement | | MW$_{heat}$ | 29.76 | 55.23 |
| heat recovery potential | | MW$_{heat}$ | 19.29 | 30.12 |
| FT crude output | | barrels/day | 696.5 | 677.3 |
| product distribution | $C_1$–$C_4$ | % | 2.8 | 2.4 |
| | naphtha ($C_5$–$C_{11}$) | | 53.4 | 53.8 |
| | diesel ($C_{12}$–$C_{19}$) | | 31.1 | 31.5 |
| | waxes (>$C_{20}$) | | 10.1 | 11.3 |
| | olefins $C_5$+ | | 1.0 | 1.1 |
| FT crude production efficiency | | % | 40.3 | 39.3 |
| ratio of carbon captured to the total carbon fed to the CLG−FT process | | | 0.640 | 0.644 |
| carbon capture capacity | | kt of $CO_2$/year | 178.6 | 179.5 |

From Table 11, it can be seen that the FT crude production efficiency (39.3−40.3%) and the ratio of carbon captured to the total carbon fed to the CLG−FT process (0.64−0.644) are relatively the same for the two cases. The heat recovery potential estimated for case CG increases by 56.1% for case HG that employs a hot-gas cleanup train, eliminating the need for an additional AGR unit in case CG.

**5.7. Discussions.** Syngas derived from high-volatile fuels generally tends to have higher $H_2$/CO ratios compared to coal-derived syngas.[66] However, the extent of gas conditioning required is still dependent upon the chosen downstream fuel synthesis process. For example, the $H_2$/CO ratio in the raw syngas, through the indirect gasification process reported in the GoBiGas plant, was around 1.6−1.7, which is shifted to ratios greater than 3.0 in a WGS reactor for the methanation process.[45] In comparison to the IG process, the $H_2$/CO ratio in the raw syngas estimated from the CLG process models is higher. In case HG with the HGCU train, it was observed that the shift reactor is bypassed in almost all cases, with varied S/B ratios. As the model uses a calculator block to split the incoming syngas stream based on the set target of a $H_2$/CO ratio of 2.0 at the FT reactor inlet. The reactor is bypassed in all cases, as the $H_2$/CO ratios are already at a higher range in the raw syngas. In addition to this, the $H_2$/CO ratio at the FT inlet becomes adjusted by the incoming recycle stream from

the ATR and the $CO_2$ removal unit. For example, in case HG, assuming a S/B ratio of 1.2, $H_2$/CO is approximately 2.08 in the raw syngas, which increases to roughly 2.49 at the FT inlet. The CLG model in case HG was tested with lower OTC of the LD slag, which expectedly resulted in a lower $H_2$/CO ratio in the raw syngas. The $H_2$/CO ratio nonetheless remains within satisfactory ratios (>2.0) at the FT inlet. These results, which are based on equilibrium conditions, indicate that the water−gas shift reactor may not be critical to the CLG−FT process with LD slag as the primary OC. It is however important to note that the extent of syngas cleaning and conditioning required in the downstream processes of the overall biomass-to-liquid fuel process chain depends upon the quality ($H_2$/CO ratios and tar and methane yields) of syngas produced in the CLG process, which is, in turn, dependent upon several factors, such as operating conditions and the type of OC and biomass feedstock used in the CLG process. Therefore, it is expected that the overall system efficiency or the FT crude production efficiency is influenced by operating conditions, type of biomass, and OCs used in the CLG process.

Some of the limitations of the developed CLG process model include the assumption of complete char conversion, active species of the OC, and calibration performed in the model for methane and tar formation. Although high char conversions (>75%) are reported in the literature on CLG operations, the assumption of complete conversion could lead to a slight overestimation of the $CO_2$ yield predicted from the model. In addition to this, the OC circulation rate predicted by the model to maintain an autothermal operation could be marginally overestimated, as there is no carbon leakage to the AR in the model. The model also limits the reduction of OC to the $Fe_2O_3$/$Fe_3O_4$ oxide couple in the volatile combustion stage, which estimates an OTC of LD slag to be around 0.963%. The estimated OTC is within the expected OTC of LD slag reported;[18,40,41] however, other active phases are expected during CLG operation.

In comparison of the GCC of case HG to that of case CG, the former is expected to have much higher excess heat available for heat and power production. However, in case HG, an intermediate operating pressure of 10 bar is chosen for the gasification stage to compensate for downstream pressure losses and to operate the WGS reactor at a higher pressure, which would require lower catalyst volumes. Challenges, such as controlling solid circulation in a pressurized system, could arise. Although economic evaluation is not performed for the two cases, it is expected that the added costs associated with the pressurized operation, such as reactor design, fuel feeding, and compression, could start competing with the expected economic gains from case HG. In addition to this, it was found that, in case CG, only a minute fraction of syngas requires gas conditioning, whereas in case HG, with the HGCU train, the gas conditioning stage may not be critical to the CLG process, which could provide additional economic gains. These competing economic factors and the economic viability of the CLG process for FT crude production with net-negative $CO_2$ emissions are explored and evaluated in part 2 (10.1021/acs.energyfuels.2c01184) of this work.

## 6. CONCLUSION

CLG for FT crude production, with two different gas cleaning process configurations, has been evaluated in this study: case CG, with a conventional cold-gas cleanup train, and case HG, with a hot-gas cleanup train, where the gasification stage

operates at ambient and intermediate (10 bar) pressures, respectively. A simplified modeling approach for the CLG process was established with LD slag as the primary OC to enable a system-level analysis of the CLG−FT process. The simulation of the CLG process showed that the production of high-energy-content syngas (12 MJ/Nm$^3$) with a high $H_2$/CO ratio is possible with net-negative $CO_2$ emissions. A high $H_2$/CO ratio (>1.6) in the raw syngas provides the added advantage of eliminating the costly gas conditioning stage prior to the downstream FTS process.

The two cases predict similar CGE of roughly 74% with a FT crude production efficiency of roughly 40%. For the CLG model sized to a thermal input of 100 MW$_{th}$ of biomass, a FT crude production capacity of roughly 677−696 barrels/day is predicted. FT crude obtained from the model is mainly comprised of naphtha (∼53%), followed by FT diesel (∼31%) and waxes (∼10%). Of the total carbon fed to the process, roughly 64% is captured for storage, corresponding to a $CO_2$ capture capacity of approximately 180 kt of $CO_2$/year. In comparison of the GCCs of cases CG and HG, excess heat available on site increases by 51.6% in the latter, providing adequate heat recovery opportunities to meet the on-site steam and electricity demand. The more suitable gas cleaning train for the integrated CLG−FT model would, however, depend upon the various competing economic costs in the overall process chain.

Sensitivity analysis was performed to analyze the effect of the S/B ratio, gasification temperature, and pressure on the gas compositions and CGE of the CLG process. For a S/B ratio of 1.0−1.2, the $H_2$/CO ratio is estimated to be above 2, suitable for the downstream FTS process to produce synthetic crude with net-negative $CO_2$ emissions. Overall, the developed CLG process model could be adapted to other OCs of interest and further developed for either integration with process industries that require sustainable reducing-gas or investigation of other fuel synthesis routes. The developed CLG model will provide a basis for future comparative techno-economic analyses for applying and integrating CLG to different downstream processes.

## ■ ASSOCIATED CONTENT

### ⓈI Supporting Information

The Supporting Information is available free of charge at https://pubs.acs.org/doi/10.1021/acs.energyfuels.2c00819.

> Main unit operators and process conditions used in the FTS model (Table S1) and detailed stream data of all of the major stream flows in the CLG−FT model (Tables S2−S5) (PDF)

## ■ AUTHOR INFORMATION

### Corresponding Author

**Tharun Roshan Kumar** − *Division of Energy Technology, Department of Space, Earth, and Environment, Chalmers University of Technology, SE-412 58 Gothenburg, Sweden;* ⓞ orcid.org/0000-0002-7425-0067; Email: tharunr@chalmers.se

### Authors

**Tobias Mattisson** − *Division of Energy Technology, Department of Space, Earth, and Environment, Chalmers University of Technology, SE-412 58 Gothenburg, Sweden;* ⓞ orcid.org/0000-0003-3942-7434

**Magnus Rydén** − *Division of Energy Technology, Department of Space, Earth, and Environment, Chalmers University of Technology, SE-412 58 Gothenburg, Sweden*

**Viktor Stenberg** − *CIT Industriell Energi AB, SE-412 58 Gothenburg, Sweden*

Complete contact information is available at:
https://pubs.acs.org/10.1021/acs.energyfuels.2c00819

### Author Contributions

Tharun Roshan Kumar, conceptualization, methodology, writing, visualization, and original draft; Tobias Mattisson, conceptualization, supervision, and writing—review and editing; Magnus Rydén, conceptualization, supervision, and writing—review and editing; and Viktor Stenberg, writing—review and editing.

### Notes

The authors declare no competing financial interest.

## ■ NOMENCLATURE

AFR = air−fuel ratio
AGR = acid gas removal
AR = air reactor
CGCU = cold-gas cleanup
DCOALIGT = IGT coal density model
DFB = dual fluidized bed
DME = dimethyl ether
EF = entrained flow
EU = European Union
Fe−Cr = iron−chromium catalyst
FICFB = fast internally circulating fluidized bed
FR = fuel reactor
FT = Fischer−Tropsch
FT crude = heavier hydrocarbon products from Fischer−Tropsch synthesis
FT diesel = long-chained hydrocarbons with a carbon number ranging from $C_{12}$ to $C_{19}$
FTS = Fischer−Tropsch synthesis
GCC = grand composite curve
GHG = greenhouse gas
GoBiGas = Gothenburg Biomass Gasification
HCOALGEN = general coal model for computing enthalpy in Aspen Plus
HEN = heat exchanger network
HGCU = hot-gas cleanup
HHV = higher heating value
HP = high pressure
HTFT = high-temperature Fischer−Tropsch
IEA = International Energy Agency
IG = indirect gasification
IGT = Institute of Gas Technology
ILUC = indirect land-use change
IPCC = Intergovernmental Panel on Climate Change
IWP = industrial wood pellets
LD = Linz−Donawitz
LDS-57 = LD slag with 43% inert sand dilution

LDS-80 = LD slag with 20% inert sand dilution

LHV = lower heating value

LP = low pressure

LTFT = low-temperature Fischer–Tropsch

MC = moisture content

MDEA = methyldiethanolamine

MDEA/PZ = methyldiethanolamine/piperazine

MEA = monoethanolamine

MP = medium pressure

naphtha = long-chained hydrocarbons with a carbon number ranging from $C_5$ to $C_{11}$

OC = oxygen carrier

OL-AA = olivine artificially activated

OTC = oxygen transport capacity

PG = purge gas

PR-BM = Peng–Robinson equation of state with Boston–Mathias modifications

RME = rapeseed methyl ester

S/B = steam/biomass ratio (mass basis)

Selexol = physical solvent made of dimethyl ethers of polyethylene glycol

SEP = separator block

SG = char–steam gasification submodel

SNG = synthetic natural gas

SYN-CLN = syngas cleaning model

WGS = water–gas shift

## Symbols

$\dot{m}$ = mass flow

$\Delta H$ = heat of reaction (kJ/mol)

$G_v$ = total syngas flow ($Nm^3/s$)

MeO = metal oxides

$n_i$ = mole fractions

$R_O$ = oxygen ratio

$X$ = conversion

$\alpha$ = mechanism factor

$\eta$ = efficiency

## Indices/Exponents/Subscripts

biomass = biomass feed on a dry and ash-free basis

ch = chemical

CO = carbon monoxide

comb = combustion

db = dry basis

daf = dry and ash-free basis

e,consumed = electricity consumed

e,net = net electricity

e,produced = electricity produced

el = electricity

f = feed

fuel = biomass fuel

$i$ = gas species

in = inlet

is = isentropic

$m$ = hydrogen atoms

min = minimum

$n$ = carbon atoms

ox = oxidized

$p$ = oxygen atoms

product = FT crude products

red = reduced

sg = syngas

sys = system

temp = temperature

th = thermal

v = standard volume ($Nm^3$)

$x$ = metal atoms in metal oxides

$y$ = oxygen atoms in metal oxides

## ■ REFERENCES

(1) International Energy Agency (IEA). *Technology Roadmap: Biofuels for Transport*; IEA: Paris, France, 2011; DOI: 10.1787/9789264118461-en.

(2) Hofbauer, H.; Rauch, R.; Veronik, G.; Fleck, T. *Gasification of Organic Material in a Novel Fluidized Bed Reactor*, 1997; p 2554.

(3) Mattisson, T.; Keller, M.; Linderholm, C.; Moldenhauer, P.; Rydén, M.; Leion, H.; Lyngfelt, A. Chemical-Looping Technologies Using Circulating Fluidized Bed Systems: Status of Development. *Fuel Process. Technol.* **2018**, *172*, 1−12.

(4) Lyngfelt, A.; Brink, A.; Langørgen, Ø.; Mattisson, T.; Rydén, M.; Linderholm, C. 11,000 h of Chemical-Looping Combustion Operation—Where Are We and Where Do We Want to Go? *Int. J. Greenhouse Gas Control* **2019**, *88*, 38−56.

(5) Lyngfelt, A.; Leckner, B. A 1000 $MW_{Th}$ Boiler Boiler for Chemical-Looping Combustion of Solid Fuels—Discussion of Design and Costs. *Appl. Energy* **2015**, *157*, 475−487.

(6) Leion, H.; Mattisson, T.; Lyngfelt, A. Solid Fuels in Chemical-Looping Combustion. *Int. J. Greenhouse Gas Control* **2008**, *2* (2), 180−193.

(7) Mattisson, T.; Lyngfelt, A.; Leion, H. Chemical-Looping with Oxygen Uncoupling for Combustion of Solid Fuels. *Int. J. Greenhouse Gas Control* **2009**, *3* (1), 11−19.

(8) Berdugo Vilches, T.; Thunman, H. Impact of Oxygen Transport on Char Conversion in Dual Fluidized Bed Systems. *Proceedings of Nordic Flame Days 2015*; Copenhagen, Denmark, Oct 6−7, 2015.

(9) Moldenhauer, P.; Linderholm, C.; Rydén, M.; Lyngfelt, A. Avoiding $CO_2$ Capture Effort and Cost for Negative $CO_2$ Emissions Using Industrial Waste in Chemical-Looping Combustion/Gasification of Biomass. *Mitig. Adapt. Strateg. Glob. Change* **2019**, *25*, 1−24.

(10) Ge, H.; Guo, W.; Shen, L.; Song, T.; Xiao, J. Biomass Gasification Using Chemical Looping in a 25 $kW_{Th}$ Reactor with Natural Hematite as Oxygen Carrier. *Chem. Eng. J.* **2016**, *286*, 174−183.

(11) Pissot, S.; Vilches, T. B.; Maric, J.; Seemann, M. Chemical Looping Gasification in a 2−4 $MW_{th}$ Dual Fluidized Bed Gasifier. *Proceedings of the 23rd International Conference on Fluidized Bed Conversion*; Seoul, South Korea, May 12−16, 2018.

(12) Jin, B.; Zhao, Y.; Fan, Y.; Deng, Z.; Liang, Z. Thermal Management for Chemical Looping Systems with Chemical Production. *Chem. Eng. Sci.* **2020**, *214*, 115431.

(13) Condori, O.; García-Labiano, F.; de Diego, L. F.; Izquierdo, M. T.; Abad, A.; Adánez, J. Biomass Chemical Looping Gasification for Syngas Production Using Ilmenite as Oxygen Carrier in a 1.5 $kW_{th}$ Unit. *Chem. Eng. J.* **2021**, *405*, 126679.

(14) Zeng, J.; Xiao, R.; Zeng, D.; Zhao, Y.; Zhang, H.; Shen, D. High $H_2$/CO Ratio Syngas Production from Chemical Looping Gasification of Sawdust in a Dual Fluidized Bed Gasifier. *Energy Fuels* **2016**, *30* (3), 1764−1770.

(15) Huseyin, S.; Wei, G.; Li, H.; He, F.; Huang, Z. Chemical-Looping Gasification of Biomass in a 10 $kW_{Th}$ Interconnected Fluidized Bed Reactor Using $Fe_2O_3/Al_2O_3$ Oxygen Carrier. *J. Fuel Chem. Technol.* **2014**, *42* (8), 922−931.

(16) Wang, L.; Feng, X.; Shen, L.; Jiang, S.; Gu, H. Carbon and Sulfur Conversion of Petroleum Coke in the Chemical Looping Gasification Process. *Energy* **2019**, *179*, 1205−1216.

(17) Moldenhauer, P.; Linderholm, C.; Rydén, M.; Lyngfelt, A. Experimental Investigation of Chemical-Looping Combustion and Chemical-Looping Gasification of Biomass-Based Fuels Using Steel Converter Slag as Oxygen Carrier. *Proceedings of the International Conference on Negative $CO_2$ Emissions*; Gothenburg, Sweden, May 22−24, 2018.

(18) Condori, O.; García-Labiano, F.; de Diego, L. F.; Izquierdo, M. T.; Abad, A.; Adánez, J. Biomass Chemical Looping Gasification for Syngas Production Using LD Slag as Oxygen Carrier in a 1.5 kW$_{th}$ Unit. *Fuel Process. Technol.* **2021**, *222*, 106963.

(19) Lin, Y.; Wang, H.; Wang, Y.; Huo, R.; Huang, Z.; Liu, M.; Wei, G.; Zhao, Z.; Li, H.; Fang, Y. Review of Biomass Chemical Looping Gasification in China. *Energy Fuels* **2020**, *34* (7), 7847−7862.

(20) Lee, J.; Kim, Y.; Lee, W.; Kim, S. Coal-Gasification Kinetics Derived from Pyrolysis in a Fluidized-Bed Reactor. *Energy* **1998**, *23* (6), 475−488.

(21) Huang, Z.; Zhang, Y.; Fu, J.; Yu, L.; Chen, M.; Liu, S.; He, F.; Chen, D.; Wei, G.; Zhao, K.; Zheng, A.; Zhao, Z.; Li, H. Chemical Looping Gasification of Biomass Char Using Iron Ore as an Oxygen Carrier. *Int. J. Hydrogen Energy* **2016**, *41* (40), 17871−17883.

(22) Gao, N.; Li, A.; Quan, C. A Novel Reforming Method for Hydrogen Production from Biomass Steam Gasification. *Bioresour. Technol.* **2009**, *100* (18), 4271−4277.

(23) Tian, H.; Siriwardane, R.; Simonyi, T.; Poston, J. Natural Ores as Oxygen Carriers in Chemical Looping Combustion. *Energy Fuels* **2013**, *27* (8), 4108−4118.

(24) Keller, M.; Leion, H.; Mattisson, T. Mechanisms of Solid Fuel Conversion by Chemical-Looping Combustion (CLC) Using Manganese Ore: Catalytic Gasification by Potassium Compounds. *Energy Technol.* **2013**, *1* (4), 273−282.

(25) Woolcock, P. J.; Brown, R. C. A Review of Cleaning Technologies for Biomass-Derived Syngas. *Biomass Bioenergy* **2013**, *52*, 54−84.

(26) Abdoulmoumine, N.; Adhikari, S.; Kulkarni, A.; Chattanathan, S. A Review on Biomass Gasification Syngas Cleanup. *Appl. Energy* **2015**, *155*, 294−307.

(27) Thunman, H.; Seemann, M.; Berdugo Vilches, T.; Maric, J.; Pallares, D.; Ström, H.; Berndes, G.; Knutsson, P.; Larsson, A.; Breitholtz, C.; Santos, O. Advanced Biofuel Production via Gasification—Lessons Learned from 200 Man-Years of Research Activity with Chalmers' Research Gasifier and the GoBiGas Demonstration Plant. *Energy Sci. Eng.* **2018**, *6* (1), 6−34.

(28) Bolhàr-Nordenkampf, M.; Rauch, R.; Bosch, K.; Aichernig, C.; Hofbauer, H. Biomass CHP Plant Güssing—Using Gasification for Power Generation. *Proceeding of the 2nd Regional Conference on Energy Technology Towards a Clean Envionnment*; Phuket, Thailand, Feb 12−14, 2003

(29) Wodołażski, A.; Smoliński, A. Modelling and Process Integration Study of Dimethyl Ether Synthesis from Syngas Derived from Biomass Gasification: Flowsheet Simulation. *Alexandria Eng. J.* **2020**, *59* (6), 4441−4448.

(30) Torres, W.; Pansare, S. S.; Goodwin, J. G. Hot Gas Removal of Tars, Ammonia, and Hydrogen Sulfide from Biomass Gasification Gas. *Catal. Rev.: Sci. Eng.* **2007**, *49* (4), 407−456.

(31) Ibarra-Gonzalez, P.; Christensen, L. P.; Rong, B. G. A Critical Review of Separation Technologies in Lignocellulosic Biomass Conversion to Liquid Transportation Fuels Production Processes. *Chem. Eng. Commun.* **2022**, *209* (4), 529−554.

(32) Steynberg, A.; Dry, M. *Fischer−Tropsch Technology*; Elsevier: Amsterdam, Netherlands, 2004; Vol. *152*.

(33) Pondini, M.; Ebert, M. Process Synthesis and Design of Low Temperature Fischer−Tropsch Crude Production from Biomass Derived Syngas. Master's Thesis, Chalmers University of Technology, Gothenburg, Sweden, 2013.

(34) de Klerk, A. Aviation Turbine Fuels through the Fischer−Tropsch Process. In *Biofuels for Aviation: Feedstocks, Technology and Implementation*; Chuck, C. J., Ed.; Elsevier: Amsterdam, Netherlands, 2016; Chapter 10, pp 241−259, DOI: 10.1016/B978-0-12-804568-8.00010-X.

(35) Thunman, H.; Berdugo Vilches, T.; Seemann, M.; Maric, J.; Vela, I. C.; Pissot, S.; Nguyen, H. N. T. Circular Use of Plastics-Transformation of Existing Petrochemical Clusters into Thermochemical Recycling Plants with 100% Plastics Recovery. *Sustainable Mater. Technol.* **2019**, *22*, e00124.

(36) Yang, S.; Qian, Y.; Yang, S. Development of Full $CO_2$ Capture Process Based on Rectisol Wash Technology. *Ind. Eng. Chem. Res.* **2016**, *55* (21), 6186−6193.

(37) Wang, Y.; Liu, M.; Dong, N.; Lin, Y.; Chang, G.; Wei, G.; Zhao, K.; Wang, X.; Zheng, A.; Zhao, Z.; Huang, Z.; Fang, Y.; Li, H. Chemical Looping Gasification of High Nitrogen Wood Waste Using a Copper Slag Oxygen Carrier Modified by Alkali and Alkaline Earth Metals. *Chem. Eng. J.* **2021**, *410* (2), 128344.

(38) Rydén, M.; Hanning, M.; Lind, F. Oxygen Carrier Aided Combustion (OCAC) of Wood Chips in a 12 MW$_{th}$ Circulating Fluidized Bed Boiler Using Steel Converter Slag as Bed Material. *Appl. Sci.* **2018**, *8* (12), 2657.

(39) Hildor, F.; Mattisson, T.; Leion, H.; Linderholm, C.; Rydén, M. Steel Converter Slag as an Oxygen Carrier in a 12 MW$_{th}$ CFB Boiler—Ash Interaction and Material Evolution. *Int. J. Greenhouse Gas Control* **2019**, *88* (March), 321−331.

(40) Störner, F.; Hildor, F.; Leion, H.; Zevenhoven, M.; Hupa, L.; Rydén, M. Potassium Ash Interactions with Oxygen Carriers Steel Converter Slag and Iron Mill Scale in Chemical-Looping Combustion of Biomass-Experimental Evaluation Using Model Compounds. *Energy Fuels* **2020**, *34* (2), 2304−2314.

(41) Hildor, F.; Leion, H.; Linderholm, C. J.; Mattisson, T. Steel Converter Slag as an Oxygen Carrier for Chemical-Looping Gasification. *Fuel Process. Technol.* **2020**, *210*, 106576.

(42) Yu, Z.; Yang, Y.; Yang, S.; Zhang, Q.; Zhao, J.; Fang, Y.; Hao, X.; Guan, G. Iron-Based Oxygen Carriers in Chemical Looping Conversions: A Review. *Carbon Resour. Convers.* **2019**, *2* (1), 23−34.

(43) Chen, H.; Zheng, Z.; Chen, Z.; Bi, X. T. Reduction of Hematite ($Fe_2O_3$) to Metallic Iron (Fe) by CO in a Micro Fluidized Bed Reaction Analyzer: A Multistep Kinetics Study. *Powder Technol.* **2017**, *316*, 410−420.

(44) Chein, R. Y.; Chen, W. H. Thermodynamic Analysis of Integrated Adiabatic Chemical Looping Combustion and Supercritical $CO_2$ Cycle. *Energy Convers. Manage.* **2020**, 113643.

(45) Alamia, A.; Larsson, A.; Breitholtz, C.; Thunman, H. Performance of Large-Scale Biomass Gasifiers in a Biorefinery, a State-of-the-Art Reference. *Int. J. Energy Res.* **2017**, *41* (14), 2001−2019.

(46) Arvidsson, M.; Heyne, S.; Morandin, M.; Harvey, S. Integration Opportunities for Substitute Natural Gas (SNG) Production in an Industrial Process Plant. *Chem. Eng. Trans.* **2012**, *29*, 331−336.

(47) Fiaschi, D.; Lombardi, L. Integrated Gasifier Combined Cycle Plant with Integrated $CO_2−H_2S$ Removal: Performance Analysis, Life Cycle Assessment and Exergetic Life Cycle Assessment. *Int. J. Appl. Thermodyn.* **2002**, *5* (1), 13−24.

(48) Doherty, W.; Reynolds, A.; Kennedy, D. Aspen Plus Simulation of Biomass Gasification in a Steam Blown Dual Fluidised Bed. *Materials and Processes for Energy: Communicating Current Research and Technological Developments*; Méndez-Vilas, A., Ed.; Formatex Research Centre: Badajoz, Spain, 2013; pp 212−220.

(49) Halvorsen, B. M.; Adhikari, U.; Eikeland, M. S. Gasification of Biomass for Production of Syngas for Biofuel. *Proceedings of the 56th Conference on Simulation and Modelling (SIMS 56)*; Linköping, Sweden, Oct 7−9, 2015; DOI: 10.3384/ecp15119255.

(50) Aspen Technology. *Aspen Physical Property System: Physical Property Methods and Models 11.1*; Aspen Technology: Cambridge, MA, 2011; pp 1−19.

(51) Song, T.; Shen, L.; Xiao, J.; Chen, D.; Gu, H.; Zhang, S. Nitrogen Transfer of Fuel-N in Chemical Looping Combustion. *Combust. Flame* **2012**, *159* (3), 1286−1295.

(52) Song, T.; Guo, W.; Shen, L. Fuel Nitrogen Conversion in Chemical Looping with Oxygen Uncoupling of Coal with a CuO-Based Oxygen Carrier. *Energy Fuels* **2015**, *29* (6), 3820−3832.

(53) Larsson, A.; Israelsson, M.; Lind, F.; Seemann, M.; Thunman, H. Using Ilmenite to Reduce the Tar Yield in a Dual Fluidized Bed Gasification System. *Energy Fuels* **2014**, *28* (4), 2632−2644.

(54) Arvidsson, M.; Morandin, M.; Harvey, S. Biomass Gasification-Based Syngas Production for a Conventional Oxo Synthesis Plant-

Process Modeling, Integration Opportunities, and Thermodynamic Performance. *Energy Fuels* **2014**, *28* (6), 4075−4087.

(55) Jerndal, E.; Mattisson, T.; Lyngfelt, A. Thermal Analysis of Chemical-Looping Combustion. *Chem. Eng. Res. Des.* **2006**, *84* (9), 795−806.

(56) Kraussler, M.; Binder, M.; Fail, S.; Bosch, K.; Hackel, M.; Hofbauer, H. Performance of a Water Gas Shift Pilot Plant Processing Product Gas from an Industrial Scale Biomass Steam Gasification Plant. *Biomass Bioenergy* **2016**, *89* (2016), 50−57.

(57) Binder, M.; Kraussler, M.; Kuba, M.; Luisser, M. *Hydrogen from Biomass Gasification*; International Energy Agency (IEA): Paris, France, 2018; IEA Bioenergy Task 33, pp 265−271.

(58) Liu, K.; Song, C.; Subramani, V. *Hydrogen and Syngas Production and Purification Technologies*; Liu, K., Song, C., Subramani, V., Eds.; John Wiley & Sons, Inc.: Hoboken, NJ, 2009; DOI: 10.1002/9780470561256.

(59) Ratnasamy, C.; Wagner, J. Water Gas Shift Catalysis. *Catal. Rev.: Sci. Eng.* **2009**, *51* (3), 325−440.

(60) Johansson, D.; Berntsson, T.; Franck, P.-Å. Integration of Fischer−Tropsch Fuel Production with a Complex Oil Refinery. *Int. J. Environ. Sustainable Dev.* **2014**, *13* (1), 50−73.

(61) Marx, F.; Dieringer, P.; Ströhle, J.; Epple, B. Design of a 1 $MW_{th}$ Pilot Plant for Chemical Looping Gasification of Biogenic Residues. *Energies* **2021**, *14* (9), 2581.

(62) Waldheim, L.; Nilsson, T. *Heating Value of Gases from Biomass Gasification*; International Energy Agency (IEA): Paris, France, 2001; IEA Bioenergy Agreement, Task 20—Thermal Gasification of Biomass, p 3.

(63) Linnhoff, B.; Flower, J. R. Synthesis of heat exchanger networks: I. Systematic generation of energy optimal networks. *AIChE J.* **1978**, *24* (4), 633−641.

(64) Kemp, I. C. Data Extraction and Energy Targeting. In *Pinch Analysis and Process Integration*, 2nd ed.; Kemp, I. C., Ed.; Butterworth-Heinemann: Oxford, U.K., 2007; Chapter 3, pp 41−98, DOI: 10.1016/B978-075068260-2.50008-0.

(65) Götz, M.; Köppel, W.; Reimert, R.; Graf, F. Optimierungspotenzial von Wäschen Zur Biogasaufbereitung Teil 2. Chemische Wäschen (Potential to Optimize Scrubbers for Biogas Cleaning Part 2. Chemical Scrubbers). *Chem. Ing. Tech.* **2012**, *84* (1−2), 81−87.

(66) Jiang, Y.; Bhattacharyya, D. Plant-Wide Modeling of an Indirect Coal-Biomass to Liquids (CBTL) Plant with $CO_2$ Capture and Storage (CCS). *Int. J. Greenhouse Gas Control* **2014**, *31*, 1−15.

## 📖 Recommended by ACS